Topology optimization of plate-like structures

by
Dineo Khoza

A dissertation submitted in partial fulfillment
of the requirements for the degree of

Master of Engineering

in the Department of Mechanical and Aeronautical Engineering,
University of Pretoria

March 2005

Supervisor:
Prof. Albert A. Groenwold

Abstract

Title: Topology optimization of plate-like structures

Author: Dineo Khoza

Supervisor: Prof. A.A. Groenwold

Department: Department of Mechanical Engineering

Degree: Master of Engineering

Keywords: Topology optimization, optimality criterion, method of moving asymptotes, finite element method, plates, shells

This thesis deals with the topology optimization of plate and shell structures. The shell structures are modeled as plate-like flat facets.

Firstly, the formulation of the topology optimization problem is presented in an introductory chapter, which introduces two frequently used topology optimization algorithms (being the optimality criterion and the method of moving asymptotes). Examples of applications are shown, and filtering schemes are introduced.

Secondly, the derivation of the finite element formulation and interpolation of plates is presented. Both a shear rigid Kirchoff plate element and a shear flexible Mindlin element are considered. The latter element uses substitute shear strains to overcome locking; hence reduced integration is not necessary, as is normally required when shear flexible plate elements are used in topology optimization. The effect of both element formulations on optimal topology is then illustrated. The results reveal the notable effect of through thickness shear on optimal topology.

Thirdly, a flat shell element is constructed by combining the plate elements with a membrane element with drilling degrees of freedom. (The membrane is not discussed in any detail.) To illustrate the topology optimization of shell structures, the so-called Scordelis-Lo roof is then selected as an example problem. The analysis includes an assessment of the effect of eccentric stiffeners or ribs on optimum topology.

Opsomming

Titel:	Topologie optimering van plaatagtige strukture
Outeur:	Dineo Khoza
Leier:	Prof. A.A. Groenwold
Departement:	Departement Meganiese Ingenieurswese
Graad:	Meester van Ingenieurswese
Sleutelwoorde:	Topologie optimering, optimaliteitskriterium, metode van bewegende asimptote, eindige element metode, plate, doppe

Hierdie verhandeling is gemoeid met die topologie optimering van plaat- en dopstrukture. Die dopstrukture word as plaatagtige plat fasette gemodeleer.

Eerstens word die formulering van die topologie optimeringsprobleem in 'n inleidende hoofstuk aangebied, terwyl twee gereeld gebruikte algoritmes in topologie optimering ook voorgestel word (naamlik die optimaliteitskriterium en die metode van bewegende asimptote). Voorbeelde van toepassings word getoon, en filter skemas word ingelei.

Tweedens word die afleiding van die eindige element formulering en interpolering van plate aangebied. Beide 'n skuif-star Kirchoff plaat element and 'n skuif-vervormbare Mindlin element word beskou. Laasgenoemde element gebruik plaasvervangende skuifvervormings om sluiting te oorkom. Die voordeel is dat verminderde integrasie van die element nie meer nodig nie, terwyl dit gewoonlik wel nodig is wanneer skuif vervormbare plaatelemente in topologie optimering gebruik word. Die effek van beide element formulerings op optimale topologie word dan aangetoon. Die resultate getuig van die waarneembare effek van deurdikte skuif op optimale topologie.

Derdens word 'n plat dop element gekonstrueer, deur samestelling van die plaat elemente en 'n membraan element met rotasionele vryheidsgrade. (Die membraan word nie in veel besonderhede bespreek nie.) Om die topologie optimering van dop strukture te illustreer, word die sogenaamde Scordelis-Lo dak dan as 'n voorbeeld uitgekies. Die analise sluit 'n bepaling van die effek van eksentriese verstywers of ribbe op optimale topologie in.

Acknowledgments

I would like to express my sincere gratitude towards the following persons:

- My family for their undying support,
- Prof. A.A. Groenwold for his invaluable input, guidance and support,
- Mr. C.S. Long for his immense contribution,
- and to all my good friends for being there throughout.

Financial support granted by the N.R.F is gratefully acknowledged.

Contents

List of Figures

List of Tables

Chapter 1

Introduction

1.1 Motivation

In recent years, computer aided topology optimization has been receiving increasing attention. It is a relatively new but rapidly expanding field of structural mechanics. It is used in an increasing rate in industrial applications, for example in the automotive, machine and aerospace industries. The reason for this is that it often achieves greater savings and design improvements than shape optimization.

In a *shape* optimization problem, the goal is to find the optimum shape of a domain, which is the 'design variable'. In a *sizing* problem, the goal may be to find the optimal thickness distribution or optimal member areas. *Topology* optimization of solid structures involves the determination of features such as the number, location and shape of holes, and the connectivity of the domain.

This thesis deals primarily with topology optimization using four node flat shell elements, formed by combining a four node assumed strain shear flexible plate element and a membrane element with drilling degrees of freedom.

Recently, there has been notable interest in the topology optimization of shell structures. Examples include the nonlinear topology optimization of layered shell structures by Stegmann and Lund [1], and the analysis and optimal design of plates and shells under dynamic loads by Falco *et al.* [2, 3].

1.2 Objectives

The longer term objective of this work is to develop an understanding of the topology optimization of structures with plates or shells to such an extent that it can be used in the development of micro-structures, such as micro electro mechanical systems (MEMS) and micro optical electro mechanical systems (MOEMS). To this intent, topology optimization algorithms and plate and flat shell finite elements are implemented in this study. An example of the topology optimization of electrostatic actuated microsystems was presented by Raulli and Maute [4].

1.3 Approach

The approach followed is to first formulate the optimization problem and the development of other required tools such as filters. To become familiar with topology optimization, a number of standard example problems are analyzed using existing algorithms frequently used in topology optimization.

Thereafter, the formulation of finite elements for plate and shell geometries is done. Both a shear rigid Kirchoff plate element and a shear flexible Mindlin element are considered. To visualize the effect of through thickness shear formulation, the plates are then used in topology optimization.

Only once basic plate problems have been studied is the progression to shell elements made. The so-called Scordelis-Lo roof is selected as the example problem. The reason for selecting this singly curved shell is that it is kinematically very interesting, since it reveals unexpected, complex kinematic behavior.

1.4 Thesis overview

In Chapter 2, a general introduction to topology optimization is given. Firstly, the formulation of the topology optimization problem, and then, different topology optimization methods, are outlined. The filtering schemes are presented and examples of their applications shown.

Chapter 3 starts with the discussion of Mindlin plate elements. The finite element interpolation is presented, followed by an assumed strain interpolation. The chapter ends off with the presentation of discrete Kirchoff quadrilateral (DKQ) plate elements.

Chapter 4 illustrates the effects of topology optimization when using both Mindlin and Kirchoff theory for flat plates. The plates are optimized for different volume fractions and different support conditions. The effect of the Poisson's ratio is also studied.

Chapter 5 presents the formulation of a general flat shell element.

Chapter 6 illustrates topology optimization using flat shell elements for the so-called Scordelis -Lo roof. The roof is optimized for different volume fractions. The penalty factor is increased in an attempt to get clearer definitions of the optimized roof. To assess the effect of curvature, a flat projection of the shell (i.e. a plate) is also studied. Finally, the effect of eccentric stiffening of the shell is also investigated.

Chapter 7 presents the study's overall conclusions and recommendations.

In Appendix A, a graphical illustration of the different filters used is given.

Appendix B gives the descriptor function sensitivities.

Appendix C tabulates some numerical results obtained for various problems.

Finally, a source code fragment of the code used is presented in Appendix D. For the sake of brevity, the finite elements used are not listed.

Chapter 2

Some typical applications of topology optimization

2.1 Problem formulation for minimum compliance

Topology optimization is an optimization technique that seeks an optimal layout discretizing the design domain, typically using the finite element method (FEM) and sensitivity analysis [5]. Simply put, the purpose of topology optimization is to find the optimal layout or material distribution of a structure within a specified region. Two algorithmic approaches are often used for solving the topology problem, namely, the optimality criterion approach [6] and the method of moving asymptotes (MMA) [7]. In topology optimization, the minimization of compliance is often sought, with relative density as the only design parameter. The applied loads, supports and the material volume are normally prescribed. The minimum compliance problem may be solved using the so-called "power-law approach". The scalar compliance c can be written as

$$c = \boldsymbol{f}^T \boldsymbol{u} = \boldsymbol{u}^T \boldsymbol{K} \boldsymbol{u} \quad , \tag{2.1}$$

where $\boldsymbol{f}$ is the global force vector, $\boldsymbol{u}$ the global displacement vector and $\boldsymbol{K}$ the global (structural) stiffness matrix of a finite element discretization of a structure.

For linear elasticity, assuming plane stress and after application of the principle of virtual work, we obtain the equilibrium equations

$$\boldsymbol{K} \boldsymbol{u} = \boldsymbol{f} \quad . \tag{2.2}$$

If the elemental stiffness matrix $\boldsymbol{K}_e$ is expressed as

$$\boldsymbol{K}_e = (x_e)^p \boldsymbol{K}_0 \quad , \tag{2.3}$$

with the design variable x_e being the relative density of the material in element e, $\boldsymbol{K}_0$ the local stiffness matrix of an element with a relative density of one, (viz. a solid element) and p a penalty factor, then the compliance may also be written as

$$c = \sum_{e=1}^{N} \boldsymbol{u}_e^T \boldsymbol{K}_e \boldsymbol{u}_e = \sum_{e=1}^{N} (x_e)^p \boldsymbol{u}_e^T \boldsymbol{K}_0 \boldsymbol{u}_e \quad . \tag{2.4}$$

Thus, a topology optimization problem formulation, where the objective is to minimize compliance, can be written as

$$\begin{aligned} \min_{\boldsymbol{x}} \quad & c(\boldsymbol{x}) = \boldsymbol{u}^T \boldsymbol{K} \boldsymbol{u} = \sum_{e=1}^{N} (x_e)^p \boldsymbol{u}_e^T \boldsymbol{K}_e \boldsymbol{u}_e \quad , \\ \text{subject to} \quad & \frac{V(\boldsymbol{x})}{V_0} = f \quad , \\ & \boldsymbol{K}\boldsymbol{u} = \boldsymbol{f} \quad , \\ & 0 < x_{min} \leq x \leq x_{max} \quad . \end{aligned} \tag{2.5}$$

Herein, $\boldsymbol{x}$ is the vector of all the densities in the elements and N is the number of elements. The lower limit, x_{min}, is greater than zero to avoid the introduction of singularities into the stiffness matrix and the upper limit, x_{max}, is of course chosen as one. The lower limit, x_{min} is normally set to a small number, e.g. 10^{-3}, to prevent numerical instabilities. fV_0 is the prescribed constraint on volume. (In compiling this chapter, we follow very closely the formulations of Pedersen and Buhl [5], Sigmund [6] and Svanberg [7].)

The penalty parameter p is introduced to penalize the intermediate density values by making their stiffness contribution to global stiffness uneconomical. Thus, the element densities prefer either of the bounds. Figure 2.1 illustrates the effect the penalty factor has on the element stiffness K_e. A higher penalty forces the intermediate densities to be penalized more.

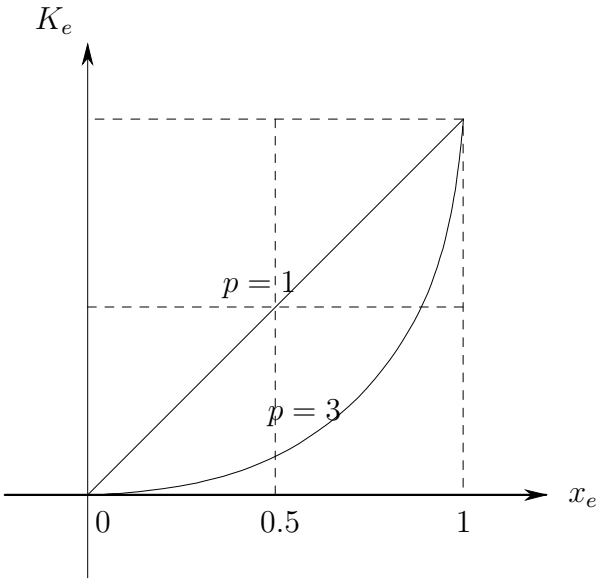

Figure 2.1: Effect of the penalty factor

2.2 The optimality criterion

The optimality criterion is a simple method frequently used for updating the design variables. It is a heuristic method based on the Lagrangian function. The Lagrangian multipliers are found through an iterative process.

The Lagrangian L for the optimization problem is given by

$$L = c + \lambda(V - fV_0) + \boldsymbol{\lambda}_1^T(\boldsymbol{K}\boldsymbol{u} - \boldsymbol{f}) + \sum_{e=1}^{N} \lambda_{2e}(x_{min} - x_e) + \sum_{e=1}^{N} \lambda_{3e}(x_e - x_{max}) \quad , \tag{2.6}$$

where λ and $\boldsymbol{\lambda}_1$ are the global Lagrangian multipliers and λ_{2e} and λ_{3e} are Lagrangian multipliers for the lower and upper side constraints.

Optimality is found when the derivatives of the Lagrangian function with respect to the design variables are zero:

$$\frac{\partial L}{\partial x_e} = 0, \quad \text{for} \quad e = 1, N \quad . \tag{2.7}$$

Hence

$$\frac{\partial L}{\partial x_e} = \frac{\partial c}{\partial x_e} + \lambda \frac{\partial V}{\partial x_e} + \boldsymbol{\lambda}_1^T \frac{\partial \boldsymbol{K}\boldsymbol{u}}{\partial x_e} - \lambda_{2e} + \lambda_{3e} \quad . \tag{2.8}$$

Assuming that the lower and upper bound constraints are not active ($\lambda_{2e} = \lambda_{3e} = 0$) and that the loads are design independent ($\frac{\partial \boldsymbol{f}}{\partial x_e} = 0$), we obtain

$$\frac{\partial L}{\partial x_e} = \frac{\partial \boldsymbol{u}^T}{\partial x_e}\boldsymbol{K}\boldsymbol{u} + \boldsymbol{u}^T\frac{\partial \boldsymbol{K}}{\partial x_e}\boldsymbol{u} + \boldsymbol{u}^T\boldsymbol{K}\frac{\partial \boldsymbol{u}}{\partial x_e} + \lambda v_e + \boldsymbol{\lambda}_1^T\left(\frac{\partial \boldsymbol{K}}{\partial x_e}\boldsymbol{u} + \boldsymbol{K}\frac{\partial \boldsymbol{u}}{\partial x_e}\right) \quad , \tag{2.9}$$

which reduces to

$$\frac{\partial L}{\partial x_e} = \boldsymbol{u}^T\frac{\partial \boldsymbol{K}}{\partial x_e}\boldsymbol{u} + \boldsymbol{\lambda}_1^T\frac{\partial \boldsymbol{K}}{\partial x_e}\boldsymbol{u} + \frac{\partial \boldsymbol{u}}{\partial x_e}(2\boldsymbol{u}^T\boldsymbol{K} + \boldsymbol{\lambda}_1^T\boldsymbol{K}) + \lambda v_e \quad . \tag{2.10}$$

Since $\boldsymbol{\lambda}_1^T$ is arbitrary, it is chosen in such a way as to eliminate the derivatives $\frac{\partial \boldsymbol{u}}{\partial x_e}$. $\boldsymbol{\lambda}_1^T$ is set equal to $-2\boldsymbol{u}^T$, to set $(2\boldsymbol{u}^T\boldsymbol{K} + \boldsymbol{\lambda}_1^T\boldsymbol{K})$ equal to zero. Hence,

$$\begin{aligned} \frac{\partial L}{\partial x_e} &= -\boldsymbol{u}^T\frac{\partial \boldsymbol{K}}{\partial x_e}\boldsymbol{u} + \lambda v_e \\ &= -p(x_e)^{p-1}\boldsymbol{u}_e^T\boldsymbol{K}_0\boldsymbol{u}_e + \lambda v_e = 0 \quad , \end{aligned} \tag{2.11}$$

where $\boldsymbol{u}_e^T\boldsymbol{K}_0\boldsymbol{u}_e$ is the energy of a solid element with density 1. Since the strain energy density should remain constant throughout the design domain, the design variables can be updated based on

$$\frac{p(x_e)^{p-1}\boldsymbol{u}_e^T\boldsymbol{K}_0\boldsymbol{u}_e}{\lambda v_e} = \frac{-\frac{\partial c}{\partial x_e}}{\lambda v_e} = B_e^k = 1 \quad . \tag{2.12}$$

The heuristic scheme for updating the design variables is then

$$x_e^{k+1} = x_e^k\left(\frac{p(x_e)^{p-1}\boldsymbol{u}_e^T\boldsymbol{K}_0\boldsymbol{u}_e}{\lambda v_e}\right)^{\zeta} = x_e^k(B_e^k)^{\zeta} \quad , \tag{2.13}$$

where ζ is the damping, which can vary from zero to one. A positive move limit m, which can also vary from zero to one, is introduced to stabilize the iteration, that is, to ensure that no big change in relative density is allowed between two successive iterations, so that an element does not go from void to solid or vice versa in one iteration. Thus, the heuristic scheme for updating the design variables then becomes

$$x_e^{k+1} = \begin{cases} max(x_{min}, x_e^k - m) & \text{if} \quad x_e^k (B_e^k)^\zeta \leq max(x_{min}, x_e^k - m) \\ x_e^k (B_e^k)^\zeta & \text{if} \quad max(x_{min}, x_e^k - m) < x_e^k (B_e^k)^\zeta < min(1, x_e^k + m) \\ min(1, x_e^k + m) & \text{if} \quad x_e^k (B_e^k)^\zeta \geq min(1, x_e^k + m) \quad . \end{cases} \tag{2.14}$$

The damping is normally set to 0.5 and again its purpose is also to stabilize the iteration. The Lagrangian multiplier is updated iteratively using bisection, such that the Lagrangian also satisfies the volume constraint.

2.3 Filters

Filters are used to prevent checkerboarding by smoothing the stiffness in a fashion similar to the filtering of an image. Filtering means that the stiffness in a point e depends on the density x_e in all points in the neighborhood of e. The method gives existence of solutions and convergence with refinement of the FE mesh. Filtering the sensitivity information of the optimization problem is an efficient way to ensure mesh-independency. Filtering works by modifying the density sensitivity of a specific element based on the weighted average of the element sensitivities in a *fixed* neighborhood.

The scheme works by modifying the element sensitivities of the compliance as

$$\frac{\partial \hat{c}}{\partial x_e} = \frac{1}{x_e \sum_{i=1}^N \hat{H}_i} \sum_{i=1}^N \hat{H}_i x_i \frac{\partial c}{\partial x_i} \quad , \tag{2.15}$$

where N is the total number of elements in the mesh and where the *mesh-independent* convolution operator (weight factor) $\hat{H}_i$ is

$$\hat{H}_i = r_{min} - dist(e, i), \quad \{i \in N \mid dist(e, i) \leq r_{min}\}, \quad e = 1, \ldots, N \quad . \tag{2.16}$$

The operator $dist(e, i)$ is the distance between the center of element e and the center of element i. The convolution operator $\hat{H}_i$ is zero outside the filter area. In the case of a *linear filter*, the convolution operator for element i decays linearly with distance from element e. Other filters that can be used are the so-called *non-linear* and *3-by-3 filters*.

The differences between the filters are illustrated in Appendix A.

2.4 Examples using the optimality criteria

In this section, some examples of topology optimization, using the optimality criterion, are shown.

2.4.1 MBB beam

The popular MBB beam is used as an example to illustrate the minimization of compliance of static structures. In Figure 2.2 the full design domain of the MBB-beam is depicted, while half the design domain with symmetry boundary conditions is shown Figure 2.3.

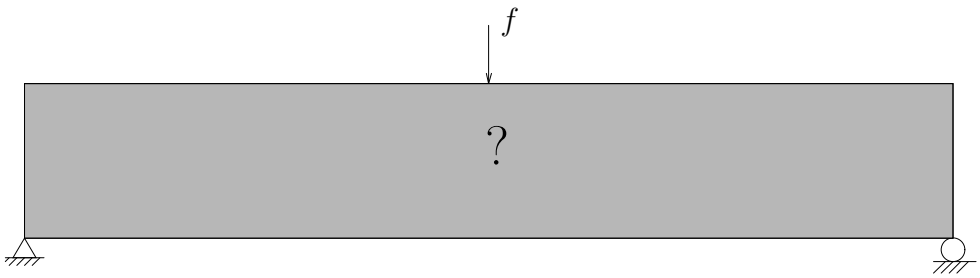

Figure 2.2: MBB beam

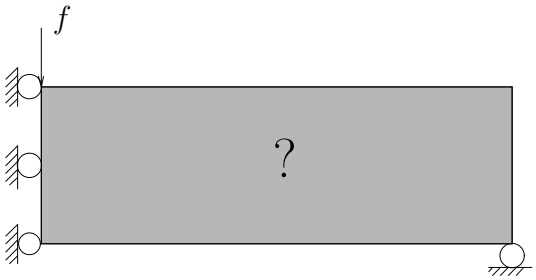

Figure 2.3: Half the MBB beam

Optimization of the MBB beam is illustrated for half the design domain with symmetry as depicted in Figure 2.3. Figure 2.4 depicts the optimized MBB-beam (using the 99 line topology optimization code developed by Sigmund [6], based on the optimality criterion presented in Section 2.2).

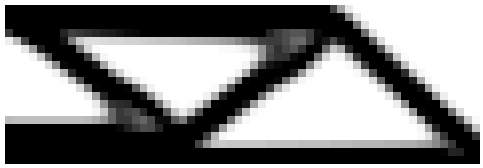

Figure 2.4: The optimized MBB beam

As indicated in the foregoing, filters are used to prevent checkerboarding. Checkerboarding is a numerical problem that yields an artificially high stiffness. Checkerboarding can also be prevented by using higher order elements (eight or nine noded elements), but the computational time may increase quite considerably. The checkerboarding effect is illustrated in Figure 2.5, which was generated without any filters.

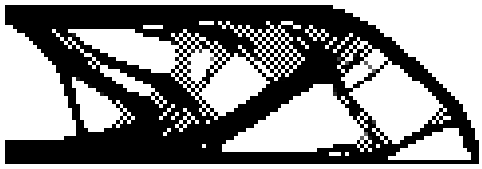

Figure 2.5: Checkerboarding of the MBB beam

Another numerical problem that can occur during topology optimization is the mesh dependency problem. This means that different solutions can be obtained for different discretizations. In Figure 2.6(a) the number of elements used is twice the number of elements used in Figure 2.6(b), with everything else the same. It is observed that the results obtained are quite different.

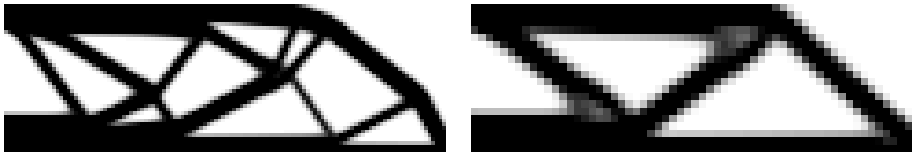

(a) *Fine mesh* (b) *Course mesh*

Figure 2.6: The optimized MBB-beam with different meshes

The mesh-dependency problem can be eliminated by giving the checkerboard filter a fixed radius as shown in Figure 2.7. The filter is independent of mesh discretization. Thus, the results obtained in Figure 2.7(a) are very similar to those obtained in Figure 2.7(b), even though the mesh discretizations used are different.

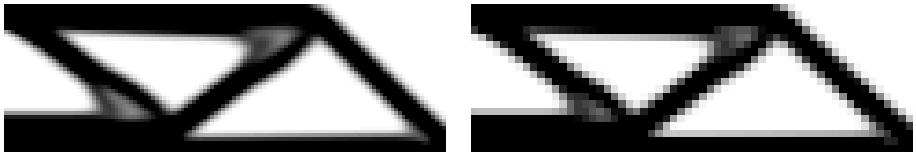

(a) *Fine Mesh* (b) *Course mesh*

Figure 2.7: An optimized MBB-beam with different mesh discretizations. (The filter used in both sub figures has the same radius)

Different solutions to the same problem with the same discretization can often be obtained just by using different starting solutions. The solution is dependent upon parameters such as move limits, damping and the penalty factor. The move limit used in Figure 2.8(b) is 0.5, as compared to the move limit of 0.2 used in Figure 2.8(a).

(a) Move limit = 0.2 (b) Move limit= 0.5

Figure 2.8: Two different move limits

2.4.2 Cantilever beam

In Figure 2.9, the domain and the boundary conditions of a cantilever beam are depicted. (This is done to illustrate the effect that different boundary conditions may have on the optimal design, as compared to the MBB beam presented in Section 2.4.1.)

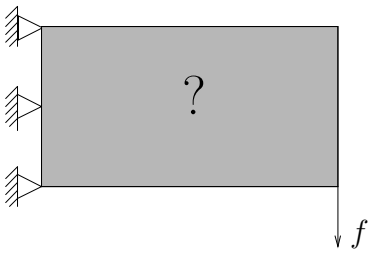

Figure 2.9: Design domain of a cantilever beam

Figure 2.10 shows the solution to the boundary condition posed in Figure 2.9.

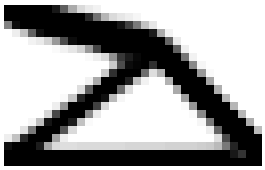

Figure 2.10: Topology optimization of a cantilever beam

In addition to applying different boundary conditions, more than one load can be applied. Figure 2.11 shows the design domain of a cantilever beam with two load cases applied to it. The solution to the problem with two load cases is presented in Figure 2.12.

In some cases, some elements may be required to take the minimum density value (e.g. due to the presence of a hole for modeling a pipe). The design domain shown in Figure 2.13 is that of a cantilever beam required to have a prescribed hole.

Passive elements can be defined for elements that are required to take the minimum or the maximum density value. The minimum density value is prescribed if a hole is required and the maximum density value prescribed if the area is required to remain solid throughout the optimization process. The solution of the cantilever beam with a fixed prescribed hole is shown in Figure 2.14.

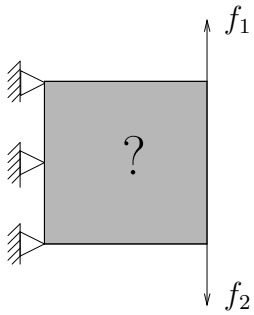

Figure 2.11: Design domain of a cantilever beam with two load cases

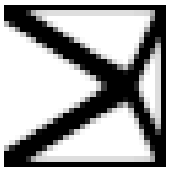

Figure 2.12: Topology optimization of a cantilever beam with two load cases

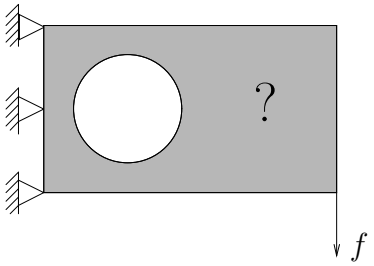

Figure 2.13: A cantilever beam with a fixed hole

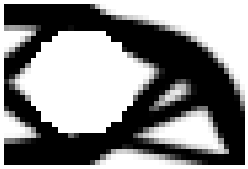

Figure 2.14: Topology optimization of a cantilever beam with a fixed hole

2.4.3 Effect of end constraints

The solution one gets from a topology optimization problem can never be better than the end constraints one imposes, i.e. different boundary constraints yield different solutions. Two loads are applied on similar structures that are constrained differently as shown in In Figure 2.15. In Figure 2.15(a), one end of the structure is fixed, while the other end is allowed to slide freely. In Figure 2.15(b), both ends of the structure are fixed.

The different results obtained in Figure 2.16(a) and Figure 2.16(b) give testimony to the

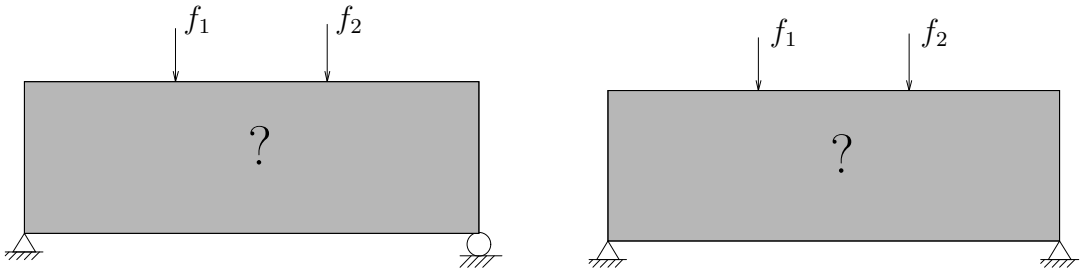

(a) Fixed-slide domain (b) Fixed-fixed domain

Figure 2.15: Differently constrained structures

fact that the solutions obtained depend on the end constraints one imposes. This means that special emphasis should be placed on ensuring that the end constraints imposed closely represent the real situation.

(a) Fixed-slide solution (b) Fixed-fixed solution

Figure 2.16: Differently constrained structures

2.5 The method of moving asymptotes (MMA)

The MMA developed by Svanberg [7] is another method that is often used for updating the design variables, where the structural optimization problem is of the form

$$\begin{aligned} \text{minimize: } & f_0(x) \\ \text{subject to: } & f_i \leq \bar{f}_i \quad , \quad i = 1, 2, ..M \\ \text{and: } & 0 < x_{min} \leq x_e \leq x_{max} \quad , \quad e = 1, 2, ..N \quad . \end{aligned} \tag{2.17}$$

Herein, M is the number of constraints and N the number of elements.

The function f_0 is the objective function and f_i the constraint functions. The implicit function f_i is approximated using the explicit functions $\tilde{f}_i^{(k)}$, with their choices based on the previously calculated function values and gradients.

The assumed approximations yield

$$\begin{aligned} \text{minimize: } & \tilde{f}_0^{(k)}(x) \\ \text{subject to: } & \tilde{f}_i^{(k)} \leq \bar{f}_i \quad , \quad i = 1, 2, ..M \\ \text{and: } & 0 < x_{min} \leq x_e \leq x_{max} \quad , \quad e = 1, 2, ..N \quad , \end{aligned} \tag{2.18}$$

where k is the number of iteration and the vector $x^{(0)}$ the starting guess for relative densities. Each approximation of the function $\tilde{f}_i^{(k)}(x)$ is obtained by a linearization of $\bar{f}_i(x)$ in the variables of the type $1/(U_e - x_e)$ or $1/(x_e - L_e)$, depending on the signs of the derivatives at $x^{(k)}$, where L_e and U_e are parameters that satisfy $L_e < x_e^{(k)} < U_e$:

$$\begin{aligned} \tilde{f}_i^{(k)}(x) &= \sum_{e=1}^{N} \left(\frac{p_{ie}}{U_e - x_e} + \frac{q_{ie}}{x_e - L_e} \right) + r_i \\ \text{if } \frac{\partial f_i}{\partial x_e} > 0 \quad \text{at} \quad x^{(k)} \quad \text{then:} \quad & p_{ie} = (U_e - x_e^k)^2 \frac{\partial f_i}{\partial x_e} \quad \wedge \quad q_{ie} = 0 \\ \text{if } \frac{\partial f_i}{\partial x_e} < 0 \quad \text{at} \quad x^{(k)} \quad \text{then:} \quad & q_{ie} = (x_e^k - L_e)^2 \frac{\partial f_i}{\partial x_e} \quad \wedge \quad p_{ie} = 0 \quad . \end{aligned} \tag{2.19}$$

r_i is chosen such that $\tilde{f}_i^{(k)}(x)^{(k)} = f_i^{(k)}(x)^{(k)}$.

The values of the asymptotic points L_e and U_e are normally changed between iterations and are given finite values. They can be updated in a heuristic way and move close to each other as the optimal design is approached. Compliance is selected for $f_0(x)$, and the structure is restricted to a prescribed fraction of the design domain, i.e. $f_1(x) = fV_0$. By using the equilibrium equations given in (2.2), the derivatives are

$$\frac{\partial \boldsymbol{K}}{\partial x_e}\boldsymbol{u} + \boldsymbol{K}\frac{\partial \boldsymbol{u}}{\partial x_e} = 0 \quad , \tag{2.20}$$

hence

$$\frac{\partial c}{\partial x_e} = \frac{\partial \boldsymbol{u}^T}{\partial x_e}\boldsymbol{K}\boldsymbol{u} \; + \; \boldsymbol{u}^T\frac{\partial \boldsymbol{K}}{\partial x_e}\boldsymbol{u} + \boldsymbol{u}^T\boldsymbol{K}\frac{\partial \boldsymbol{u}}{\partial x_e} \quad = -p(x_e)^{p-1}\boldsymbol{u}_e^T\boldsymbol{K}_0\boldsymbol{u}_e \quad , \tag{2.21}$$

in which we also assume that the loads are design independent, i.e. $\frac{\partial \boldsymbol{f}}{\partial x_e} = 0$. The derivative of the constraint function is

$$\frac{\partial V}{\partial x_e} = v_e \quad . \tag{2.22}$$

The big advantage of using MMA is that in MMA, the approximation $\tilde{f}_i^{(k)}$ is convex, and close to the behavior of the objective and constraint functions. It also allows for the solving of more complex problems with more than one constraint.

2.6 Examples using MMA

In this section, some of the capabilities of optimization using the MMA algorithm are shown, using the MMA code developed by Kristver Svanberg [7]. The MBB beam depicted in Figure 2.3 is used once again as an example to illustrate the minimization of compliance of static structures.

The MBB beam optimized using MMA is depicted in Figure 2.17. Here, the filter has the same radius as that used in Figure 2.7, with a penalty parameter and a mesh equal to that in Figure 2.7(a).

Figure 2.17: An optimized MBB-beam using MMA

The effects of the different filters is illustrated in Figure 2.18(a), Figure 2.18(b) and Figure 2.18(c). A *linear* filter is used in Figure 2.18(a). A *non-linear* filter is used in Figure 2.18(b). In Figure 2.18(c), a *3-by-3* filter is used. *No filter* is used in Figure 2.18(d) and the checkerboarding effect is very evident.

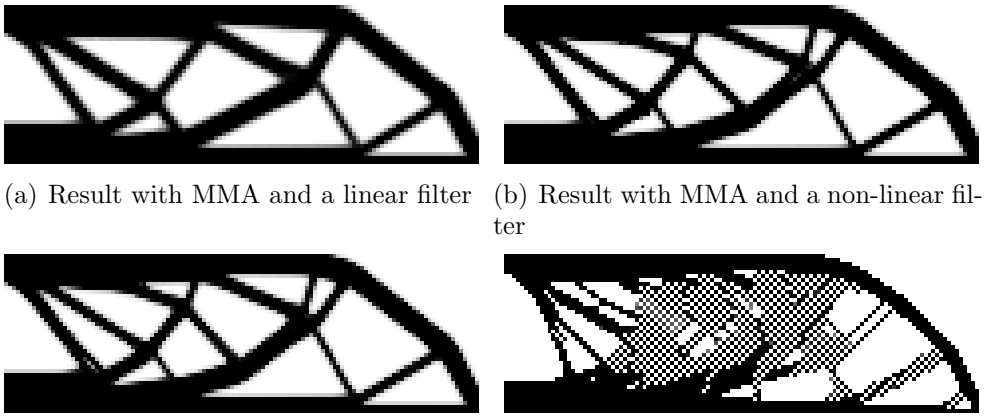

(a) Result with MMA and a linear filter

(b) Result with MMA and a non-linear filter

(c) Result with MMA and a 3-by-3 Filter

(d) Result with MMA and no filter

Figure 2.18: Results with MMA and different filters for the MBB beam

The filters in Figure 2.18 have all been applied to the sensitivities. The filters can however also be used to filter densities.

2.7 The Poulsen scheme to prevent checkerboard patterns and one-node connected hinges

A simple scheme to prevent checkerboard patterns and one-node connected hinges in topology optimization, was proposed by Poulsen [8]. The scheme is particularly important to overcome *one-node connected hinges* that are often seen in the topology optimization of compliant mechanisms, since checkerboarding effects can of course also be removed through the use of normal filters. By a one-node connected hinge it is understood that four elements surround a node, and only two opposing elements are filled with material, while the other two opposing elements are empty. These one-node connected hinges are of course also the building blocks of checkerboard patterns.

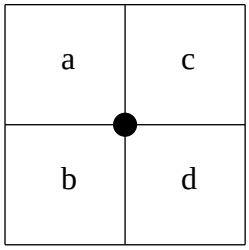

Figure 2.19: A node surrounded by 4 elements

Consider a design domain discretized by $n \times m$ elements, with the material densities x_{ij}, constant over each element e_{ij}.

The local function, h, that detects a one-node connected hinge as a function of the four elements surrounding a node in the interior of the design is defined as

$$h(a,b,c,d) = m(a,b,d).m(a,c,d).m(b,a,c).m(b,d,c) \quad , \tag{2.23}$$

where a, b, c and d are the material densities of the elements surrounding the node in question. m is defined as

$$m(a,b,c) = |b-a| + |c-b| - |c-a| \quad . \tag{2.24}$$

A one-node connected hinge has a characteristic that it is not *quasi monotonic* about the node. The function m in (2.24) detects the monotonicity of an ordered triple.

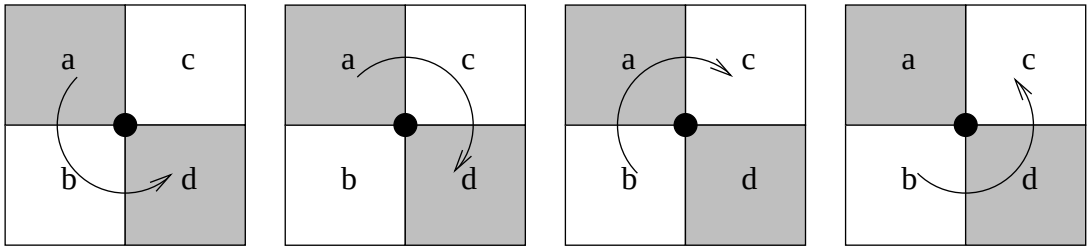

Figure 2.20: Four paths to check for quasi-monotonicity

A descriptor function for the whole design is defined as

$$H(\rho) = \sum_{j=1}^{m-1} \sum_{i=1}^{n-1} h(x_{ij}, x_{i+1j}, x_{ij+1}, x_{i+1j+1}) \quad , \tag{2.25}$$

H is zero if there are no one-node connected hinges in the design, nor any checkerboard patterns. This can be considered as an extra constraint on the design problem, e.g.

$$\min_{\rho_{ij}} \qquad \boldsymbol{u}^T \boldsymbol{K} \boldsymbol{u}$$

$$\begin{aligned} \text{subject to} \quad & \boldsymbol{K}\boldsymbol{u} = \boldsymbol{f} \\ & \Sigma_{i.j} x_{ij} s_{ij} \leq \bar{V} \\ & x_{min} \leq x_{ij} \leq 1 \\ & H(\rho) \leq \delta \quad . \end{aligned} \tag{2.26}$$

$\boldsymbol{K}$ is the stiffness matrix that depends on ρ, s_{ij} is the volume of the element e_{ij}, and $\bar{V}$ is the total volume allowed.

The sensitivity of the descriptor function is

$$\frac{dH}{de_{ij}}(\rho) = \sum_{ii=max(i-1,1)}^{min(i,n-1)} \sum_{jj=max(j-1,1)}^{min(j,m-1)} h_{,k}(d_{iijj}, d_{ii+1jj}, d_{iiij+1}, d_{ii+1ij+1}) \quad , \tag{2.27}$$

where $k = i - ii + 2(j - jj) + 1$. The computation of the sensitivities for the descriptor function is given in Appendix B.

2.8 Compliant mechanisms

In designing compliant mechanisms, the objective is typically to obtain the maximum force, $\boldsymbol{f}_2$, at the output, therefore to maximize the displacement at the output, $\boldsymbol{u}_{out}$. The subscripts 1, 2, etc. are assigned to the different design load application or displacement points (input(s) and output(s)). The displacement of the output can be written as

$$\boldsymbol{u}_{out} = \boldsymbol{f}_2^T \boldsymbol{u}_1 \tag{2.28}$$

and the optimization problem as

$$\begin{aligned} \min_{\boldsymbol{x}} \quad & \boldsymbol{u}_{out}(\boldsymbol{x}) = \boldsymbol{f}_2^T \boldsymbol{u}_1 \\ \text{subject to} \quad & \frac{V(\boldsymbol{x})}{V_0} = f \\ & \boldsymbol{K}\boldsymbol{u} = \boldsymbol{f} \\ & 0 < x_{min} \leq x \leq x_{max} \quad , \end{aligned} \tag{2.29}$$

where $x_{max} = 1$.

The expression for the sensitivities is dependent on the solution to the adjoint load case. The sensitivity of displacements for

$$\boldsymbol{K}\boldsymbol{u}_1 = \boldsymbol{f}_1 \quad ,$$

is

$$\frac{\partial \boldsymbol{K}}{\partial x_e}\boldsymbol{u}_1 + \boldsymbol{K}\frac{\partial \boldsymbol{u}_1}{\partial x_e} = \frac{\partial \boldsymbol{f}_1}{\partial x_e} = 0 \quad ,$$

hence

$$\frac{\partial \boldsymbol{u}_1}{\partial x_e} = -\boldsymbol{K}^{-1}\frac{\partial \boldsymbol{K}}{\partial x_e}\boldsymbol{u}_1 \quad . \tag{2.30}$$

To extract $\frac{\partial \boldsymbol{u}_{out}}{\partial x_e}$, the vector $\boldsymbol{f}_2$ is used:

$$\frac{\partial \boldsymbol{u}_{out}}{\partial x_e} = \boldsymbol{f}_2^T\frac{\partial \boldsymbol{u}_1}{\partial x_e} \quad . \tag{2.31}$$

Substituting (2.30) into (2.31) yields

$$\frac{\partial \boldsymbol{u}_{out}}{\partial x_e} = \boldsymbol{f}_2^T - \boldsymbol{K}^{-1}\frac{\partial \boldsymbol{K}}{\partial x_e}\boldsymbol{u}_1 = -\boldsymbol{u}_2^T\frac{\partial \boldsymbol{K}}{\partial x_e}\boldsymbol{u}_1 \quad . \tag{2.32}$$

With the penalization method used as in (2.3), this results in

$$\frac{\partial \boldsymbol{u}_{out}}{\partial x_e} = -p(x_e)^{p-1}\boldsymbol{u}_{2e}^T\boldsymbol{K}_0\boldsymbol{u}_{1e} \quad . \tag{2.33}$$

2.8.1 Force inverter

An example of a compliant mechanism synthesis is so-called force inverter.

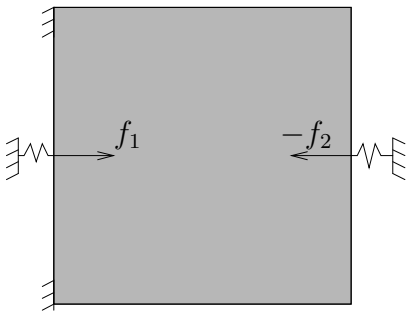

Figure 2.21: The design domain for a force inverter

Figure 2.21 gives the design domain for the force inverter and Figure 2.22 the solutions obtained with the optimality criterion and with MMA. The solutions compare closely.

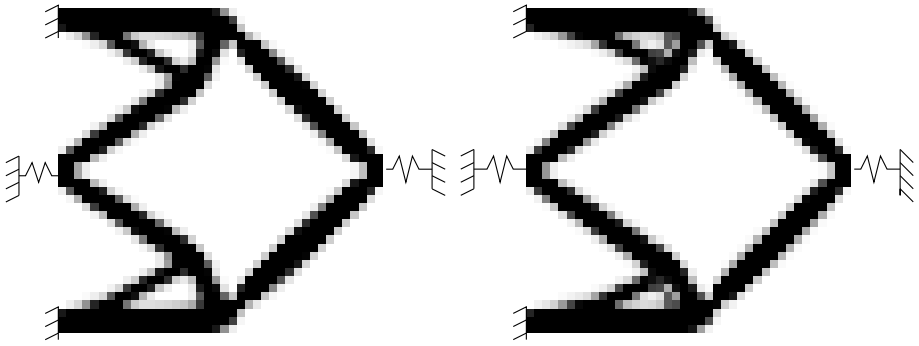

(a) *Optimality criterion* (b) *MMA*

Figure 2.22: Force inverter

2.8.2 The gripper

Another example of a compliant mechanism synthesis is the so-called 'gripper'.

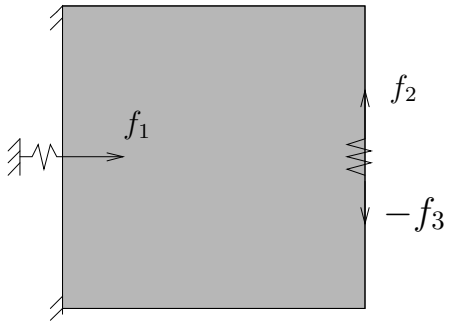

Figure 2.23: The design domain for the gripper

Figure 2.23 gives the design domain of the gripper, and Figure 2.24 the solutions obtained with the optimality criterion and with MMA. Again, the solutions compare reasonably closely.

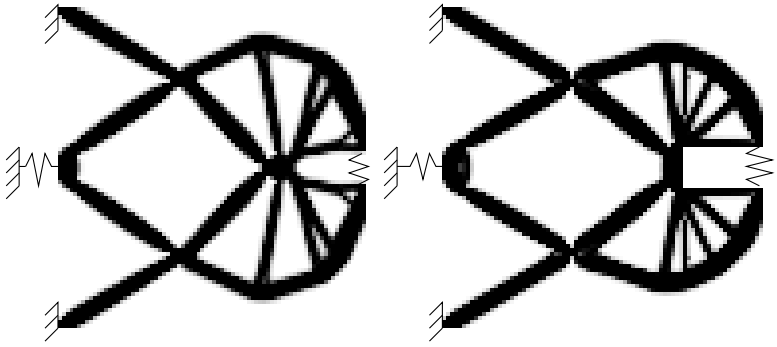

(a) *Optimality criterion* (b) *MMA*

Figure 2.24: The gripper

Chapter 3

Finite element formulation of plates

In this chapter, the finite element formulation of both Kirchoff and Mindlin plates is discussed, before they are used in Chapter 4 in actual plate topology optimization problems. (Since Kirchoff plates are often used and well known in topology optimization, I present only the interpolation of Mindlin elements.)

3.1 Assumed strain Mindlin plate elements

Firstly, plate bending elements based on the first order shear deformation theory of Mindlin-Reissner, and the assumed strain element presented by Bathe and Dvorkin [9] in particular, are discussed. This section starts with a brief discussion of 4-node plate elements and the effect of shear locking, whereafter the variational formulation and finite element interpolation of the element is presented.

3.1.1 Introduction

Due to their inherent simplicity, 4-node quadrilateral plate finite elements are very attractive. Plate elements based on the discrete Kirchhoff-Love theory are not suitable for orthotropic materials, or for isotropic problems where the contribution of transverse shear deformations are significant. The simplest suitable elements are based on the first order shear deformation theory of Mindlin and Reissner.

However, Mindlin-Reissner based 4-node plate (or shell) elements derived from the *degenerated shell* approach of Ahmad *et al.* [10] are prone to severe locking. Locking is only overcome when the element thickness is greater than an element side length. This defies the reason for the formulation of plate and shell elements, namely that the element thickness is much less than an element side length. The locking behavior is associated with the transverse shear stiffness formulation.

While transverse shear locking is avoided in elements based on the Kirchhoff-Love theory, elements based on the Mindlin-Reissner theory require modifications to alleviate shear locking. Shear locking was overcome in a number of elements through the use of reduced or selec-

tively reduced integration schemes. For the selectively reduced formulations, the transverse shear stiffness terms are evaluated with a reduced integration scheme, while full integration is retained over the part of the element stiffness associated with bending behavior.

For the 4-node plate bending elements, reduced and selective reduced integration schemes however result in the appearance of *spurious zero energy modes*. A number of elements with stabilization methods overcame this problem, of which the best known possibly are the formulations of Belytschko and co-workers. Some of these elements however require undesirable adjustable parameters, e.g. see [11, 12]. Although the elements presented by Belytschko and his co-workers are reported to be highly accurate, it seems desirable to use alternative methods (e.g. assumed strain methods) instead of the more fragile stabilization methods of Belytschko and co-workers.

In particular, the assumed strain formulation of Bathe and Dvorkin [9, 13] is considered here.

Numerical results obtained with the Bathe-Dvorkin element are readily available in the literature and are not reiterated in this study. The behavior of the Bathe-Dvorkin assumed strain plate element is summarized as follows [9]:

1. The element does not lock in thin plate analysis, i.e. the Kirchhoff hypothesis of zero transverse strains in the limit of zero thickness holds.
2. The element contains no spurious energy modes.
3. The formulation includes no numerically adjusted factors.
4. The appropriate patch tests are passed, i.e. the element is convergent.
5. The element has good predictive capabilities and is reasonably insensitive to element distortions.
6. The element is reasonably simple and inexpensive.

3.1.2 Mindlin-Reissner plates: Bending theory and variational formulation

In this section the treatments of Hinton and Huang [14] and Papadopoulos and Taylor [15] are followed, albeit with different notations. However, the same may be found in the standard works of for instance Bathe [16], Zienkiewicz and Taylor [17] and Hughes [18].

The simplest plate formulation which accounts for the effect of shear deformation, is presented. (The transverse shear is assumed constant throughout the thickness.) The assumptions of the first order Mindlin-Reissner theory are

$$\sigma_{zz} \;=\; 0 \tag{3.1}$$

$$u \;=\; z\theta_x(x,y)\;; \quad v \;=\; z\theta_y(x,y)\;; \quad w \;=\; w(x,y) \quad , \tag{3.2}$$

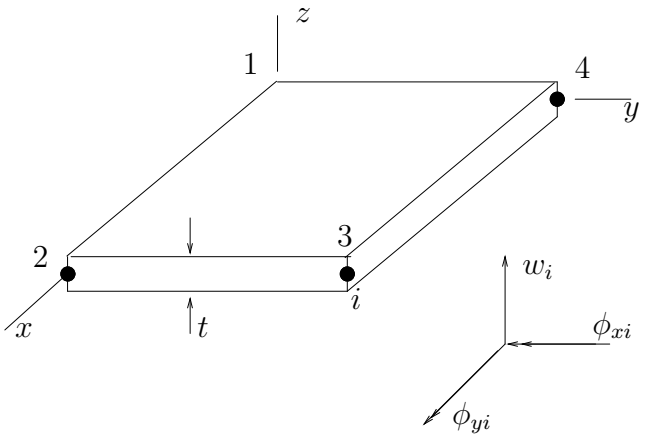

Figure 3.1: A plate element with conner nodes showing typical nodal d.o.f.

where u, v, and w are the displacements components in the x, y, and z directions respectively, w is the lateral displacement and θ_x and θ_y are the normal rotations in the xz and yz planes respectively (Figure 3.1).The element is assumed to be flat, with thickness t. (Flatness of the plate is not a necessary assumption, but merely simplifies the required notation.) The element area is denoted Ω.

Equation (3.1) is obviously inconsistent with three-dimensional elasticity. However, the transverse normal stress may be neglected for plates where the thickness is small compared with the other dimensions. Moreover, when a linear or constant through-the-thickness displacement assumption is made (as is customary in the shear-deformable plate and shell theories) limited locking occurs due to the Poisson effect, when σ_{zz} is restrained.

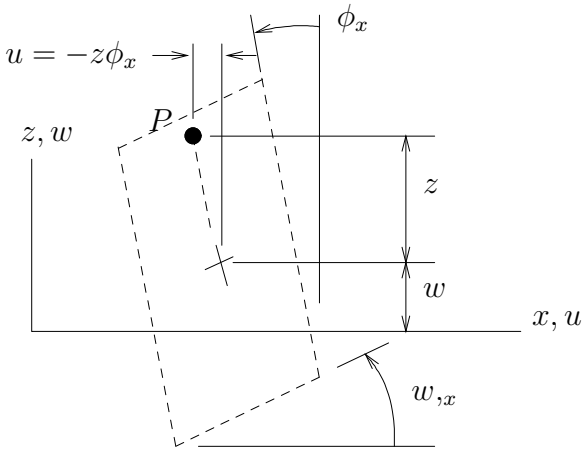

Figure 3.2: A deformed plate cross section, viewed in the +y direction.

Equations (3.2) imply that straight normals to the reference surface, ($z = 0$), remain straight, but do not necessarily remain normal to the plate after deformation (Figure 3.2). Also, the transverse displacement w is constant through the thickness.

The displacement field assumed in Equation (3.2) yields in-plane strains of the form

$$\epsilon_{xx} = z\theta_{x,x} \ , \quad \epsilon_{yy} = z\theta_{y,y} \ , \quad \gamma_{xy} = z(\theta_{x,y} + \theta_{y,x}) \quad , \tag{3.3}$$

where $\theta_{x,x} = \partial\theta_x/\partial x$, etc. The transverse shear strains are obtained as

$$\gamma_{xz} = w_{,x} + \theta_x \ , \quad \gamma_{yz} = w_{,y} + \theta_y \quad . \tag{3.4}$$

For plane stress and linear isotropic elasticity, the foregoing strain field defines the in-plane stresses as

$$\sigma_{xx} = \frac{E}{1-\nu^2}[\epsilon_{xx} + \nu\epsilon_{yy}] \quad , \tag{3.5}$$

$$\sigma_{yy} = \frac{E}{1-\nu^2}[\epsilon_{yy} + \nu\epsilon_{xx}] \quad , \tag{3.6}$$

$$\sigma_{xy} = \sigma_{yx} = G\gamma_{xy} \quad , \tag{3.7}$$

where E is Young's modulus and ν is Poisson's ratio. Similarly, the out-of-plane stresses are given by

$$\sigma_{xz} = \sigma_{zx} = G\gamma_{xz} \quad , \tag{3.8}$$

$$\sigma_{yz} = \sigma_{zy} = G\gamma_{yz} \quad , \tag{3.9}$$

where $G = E/2(1+\nu)$. Integrating the in-plane stresses, which vary linearly along the plate thickness, gives stress resultants of the form

$$M_{xx} = \int_{-t/2}^{t/2} \sigma_{xx} z \ dz \quad , \tag{3.10}$$

$$M_{yy} = \int_{-t/2}^{t/2} \sigma_{yy} z \ dz \quad , \tag{3.11}$$

$$M_{xy} = M_{yx} = \int_{-t/2}^{t/2} \sigma_{xy} z \ dz \quad . \tag{3.12}$$

Introducing matrix notation, the foregoing are written as

$$\boldsymbol{M} = [M_{xx} \ \ M_{yy} \ \ M_{xy}]^T \quad , \tag{3.13}$$

and the curvatures $\boldsymbol{\kappa}$ as

$$\boldsymbol{\kappa} = [\theta_{x,x} \ \ \theta_{y,y} \ \ \theta_{x,y} + \theta_{y,x}]^T \quad . \tag{3.14}$$

It follows that the moment-curvature relation may be expressed as

$$\boldsymbol{M} = \boldsymbol{D}_b\boldsymbol{\kappa} \quad , \tag{3.15}$$

where

$$\boldsymbol{D}_b = \frac{Et^3}{12(1-\nu^2)} \begin{bmatrix} 1 & \nu & 0 \\ \nu & 1 & 0 \\ 0 & 0 & (1-\nu)/2 \end{bmatrix} \quad . \tag{3.16}$$

Similarly, the out-of plane stresses, when integrated along the thickness, give transverse shear forces

$$Q_{xz} = \int_{-t/2}^{t/2} \sigma_{xz}\, dz \quad , \tag{3.17}$$

$$Q_{yz} = \int_{-t/2}^{t/2} \sigma_{yz}\, dz \quad , \tag{3.18}$$

which, using matrix notation, results in

$$\boldsymbol{Q} = \boldsymbol{D}_s \boldsymbol{\gamma} \quad , \tag{3.19}$$

where

$$\boldsymbol{Q} = [Q_{xz} \;\; Q_{yz}]^T \; , \quad \boldsymbol{\gamma} = [w_{,x} + \theta_x \;\; w_{,y} + \theta_y]^T \quad , \tag{3.20}$$

and

$$\boldsymbol{D}_s = Gt \begin{bmatrix} 1 & 0 \\ 0 & 1 \end{bmatrix} \quad . \tag{3.21}$$

Summation convention is implied over x, y, z for Latin indices and over x, y for Greek indices, so that the local equilibrium equations may be appropriately integrated through the thickness to deduce the plate equilibrium equations

$$M_{\alpha\beta,\beta} - S_\alpha = 0 \; ; \quad S_{\alpha,\alpha} + p = 0 \quad , \tag{3.22}$$

where p denotes the transverse surface loading. The first equation relates the bending moments to the shear forces, whereas the second is a statement of transverse force equilibrium.

In the limiting case where $t \to 0$ the Kirchhoff hypothesis of zero transverse shear strains must hold. Hence

$$w_{,x} + \theta_x = 0 \; ; \quad w_{,y} + \theta_y = 0 \quad . \tag{3.23}$$

Equations (3.4) imply that the transverse shear strain remains constant through the element thickness. This is inconsistent with classical theory, where the corresponding transverse shear stress varies quadratically. Also, the transverse shear strain on the plate surface is required to be zero. Consequently, a temporary modification to the displacement field is made, namely

$$u = z\theta_x + (z^3 + \beta z)\phi(x, y) \quad . \tag{3.24}$$

Imposing the constraint

$$\int_{-t/2}^{t/2} (z^3 + \beta z) z \, dz = 0 \quad , \tag{3.25}$$

and setting $\gamma_{xz} = 0$ on the plate faces results in

$$\gamma_{xz} = \left[1 - \frac{5}{3t^2}\left(3z^2 - \frac{3t^2}{20}\right)\right](\theta_x + w_{,x}) \quad . \tag{3.26}$$

Moreover, substituting Equation (3.26) into Equation (3.19) leads to

$$\begin{aligned} Q_{xz} &= \int_{-t/2}^{t/2} G\gamma_{xz}\, dz \\ &= G(\theta_x + w_{,x}) \int_{-t/2}^{t/2} \left[1 - \frac{5}{3t^2}\left(3z^2 - \frac{3t^2}{20}\right)\right] dz \\ &= \frac{5}{6} G(\theta_x + w_{,x}) \quad , \end{aligned} \tag{3.27}$$

Hence, for consistency reasons, a 'shear correction' term is introduced as

$$k = \frac{6}{5} \quad , \tag{3.28}$$

into Equation (3.19), which now becomes

$$\boldsymbol{Q} = \bar{\boldsymbol{D}}_s \boldsymbol{\gamma} \quad , \tag{3.29}$$

where

$$\bar{\boldsymbol{D}}_s = \boldsymbol{D}_s / k \quad . \tag{3.30}$$

The total plate energy, based on potential energy for bending and shear, is written as

$$\Pi = \frac{1}{2}\int_\Omega \boldsymbol{\kappa}^T \boldsymbol{D}_b \boldsymbol{\kappa}\, d\Omega + \frac{1}{2}\int_\Omega \boldsymbol{\gamma}^T \bar{\boldsymbol{D}}_s \boldsymbol{\gamma}\, d\Omega - \Pi_{ext} \quad , \tag{3.31}$$

where Π_{ext} is the potential energy of the applied loads. The thin plate Kirchhoff conditions of Equations (3.23) should be satisfied in the finite element interpolation.

3.1.3 Finite element interpolation

Again consider Figure 3.1. The reference surface of the element is defined by

$$\boldsymbol{x} = \sum_{i=1}^{4} N_i^e(r,s)\boldsymbol{x}_i \quad , \tag{3.32}$$

where $\boldsymbol{x}$ represents co-ordinates (x_1, x_2) and $N_i^e(r,s)$ are the isoparametric shape functions (e.g. see [19])

$$N_i^e(r,s) = \frac{1}{4}(1 + r_i r)(1 + s_i s) \; ; \; i = 1,2,3,4 \quad . \tag{3.33}$$

The sectional (normal) rotations are interpolated as

$$\theta_x = \sum_{i=1}^{4} N_i^e(r,s)\theta_{xi} \quad , \tag{3.34}$$

$$\theta_y = \sum_{i=1}^{4} N_i^e(r,s)\theta_{yi} \quad , \tag{3.35}$$

and the transverse mid-surface displacements are interpolated as

$$w = \sum_{i=1}^{4} N_i^e(r,s)w_i \quad , \tag{3.36}$$

where w_i, θ_{xi} and θ_{yi} are the nodal point values of the variables w, θ_x and θ_y respectively. The curvature-displacement relations are now written as

$$\boldsymbol{\kappa} = \sum_{i=1}^{4} \boldsymbol{B}_{bi}\boldsymbol{q}_i \quad , \tag{3.37}$$

where the element curvature-displacement matrix at node i is written as

$$\boldsymbol{B}_{bi} = \begin{bmatrix} 0 & N_{i,x}^e & 0 \\ 0 & 0 & N_{i,y}^e \\ 0 & N_{i,y}^e & N_{i,x}^e \end{bmatrix} \quad , \tag{3.38}$$

and the unknowns at node i are

$$\boldsymbol{q}_i = [w_i \;\; \theta_{xi} \;\; \theta_{yi}]^T \quad . \tag{3.39}$$

The separately interpolated curvature-displacement relationship is easily extended by the addition of a hierarchical bubble interpolation function

$$N_5(r,s) = (1-r^2)(1-s^2) \quad . \tag{3.40}$$

The terms in the element stiffness matrix arising from this interpolation may be eliminated at the element level by static condensation, e.g. see [20].

The shear strain-displacement relations are written as

$$\boldsymbol{\gamma} = \sum_{i=1}^{4} \boldsymbol{B}_{si}\boldsymbol{q}_i \quad , \tag{3.41}$$

where the element shear strain-displacement matrix at node i is written as

$$\boldsymbol{B}_{si} = \begin{bmatrix} N_{i,x}^e & N_i^e & 0 \\ N_{i,y}^e & 0 & N_i^e \end{bmatrix} \quad . \tag{3.42}$$

3.1.4 Substitute assumed strain interpolations

From the stationary condition of variational expression (3.31) the plate stiffness-displacement relationship is obtained as

$$\boldsymbol{K}^e\boldsymbol{q} \;=\; \boldsymbol{f} \quad , \tag{3.43}$$

where

$$\boldsymbol{K}^e \;=\; \boldsymbol{K}_b + \boldsymbol{K}_s \quad , \tag{3.44}$$

while

$$\boldsymbol{K}_b = \int \boldsymbol{\kappa}^T \boldsymbol{D}_b \boldsymbol{\kappa} \; d\Omega \quad , \tag{3.45}$$

and

$$\boldsymbol{K}_s = \int \boldsymbol{\gamma}^T \bar{\boldsymbol{D}}_s \boldsymbol{\gamma} \; d\Omega \quad . \tag{3.46}$$

For elements with 4 nodes, the expression for $\boldsymbol{K}_b$ is problem free (at least in terms of locking). The employed interpolation field of Equation (3.33) in $\boldsymbol{K}_s$ results in severe locking.

One solution that overcomes the locking phenomena, while ensuring that the final element formulation is rank sufficient, is to incorporate the substitute assumed strain interpolation field of Bathe and Dvorkin [9, 13].

Depicted in Figure 3.3, the assumed interpolation field of Bathe and Dvorkin is written as

$$\bar{\epsilon}_{rt} = 1/2(1+s)\bar{\epsilon}^A_{rt} + 1/2(1-s)\bar{\epsilon}^C_{rt} \tag{3.47}$$

$$\bar{\epsilon}_{st} = 1/2(1+r)\bar{\epsilon}^D_{st} + 1/2(1-r)\bar{\epsilon}^B_{st} \quad , \tag{3.48}$$

where the superscripts $A-D$ designate the sampling points for calculating the covariant shear strains. The shear strain components in the Cartesian coordinate system, $\bar{\epsilon}_{xz}$ and $\bar{\epsilon}_{yz}$ are obtained [21] using a transformation which in the case of a flat plate element reduces to the standard (2 x 2) Jacobian $\boldsymbol{J}$.

$$\left\{ \begin{array}{c} \bar{\epsilon}_{rt} \\ \bar{\epsilon}_{st} \end{array} \right\} = t/2 \left[\begin{array}{cc} x_{,r} & y_{,r} \\ x_{,s} & y_{,s} \end{array} \right] \left\{ \begin{array}{c} \bar{\epsilon}_{xz} \\ \bar{\epsilon}_{yz} \end{array} \right\} = t/2 \boldsymbol{J} \bar{\boldsymbol{\epsilon}}_s \quad . \tag{3.49}$$

Hence, the substitute shear strains $\bar{\boldsymbol{\epsilon}}_s$ are expressed as

$$\bar{\boldsymbol{\gamma}} = \bar{\boldsymbol{B}}_s \boldsymbol{q} \quad , \tag{3.50}$$

while the associated transverse stiffness-displacement relationship becomes

$$\bar{\boldsymbol{K}}_s = \int \bar{\boldsymbol{B}}_s^T \bar{\boldsymbol{D}}_s \bar{\boldsymbol{B}}_s \; d\Omega \quad . \tag{3.51}$$

The element stiffness-displacement relationship now becomes

$$(\boldsymbol{K}_b + \bar{\boldsymbol{K}}_s)\boldsymbol{q} = \boldsymbol{f} \quad , \tag{3.52}$$

which is the final element formulation. The assumed strain interpolation satisfies the Kirchhoff requirements for thin plates.

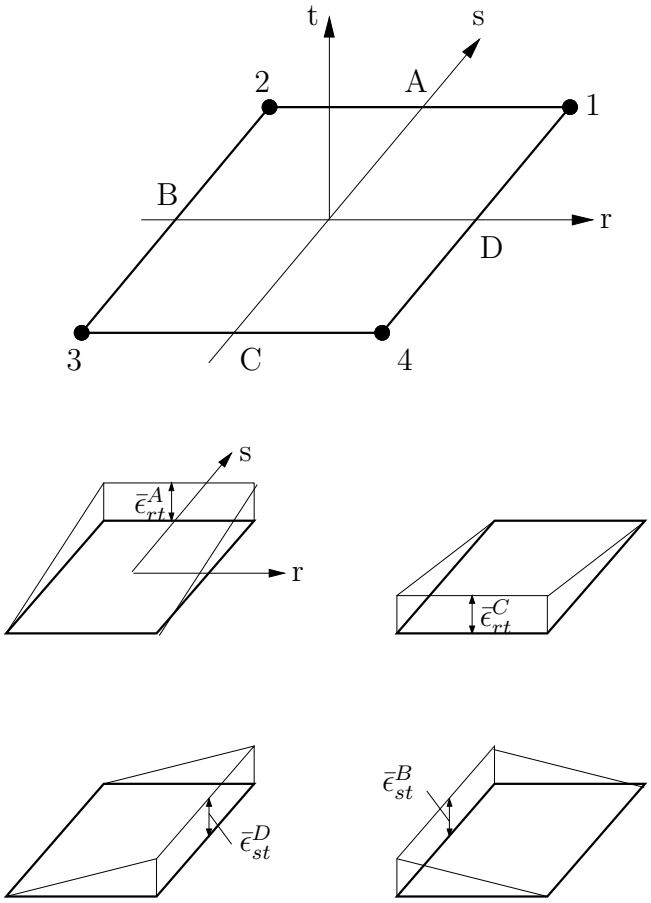

Figure 3.3: Interpolation functions for transverse shear strains

3.2 Discrete Kirchoff quadrilateral plate elements

In Kirchoff plate theory [22], transverse shear deformation is prohibited, therefore $w_{,x} = -\theta_x$ and $w_{,y} = -\theta_y$. Hence $\epsilon_{xx} = -zw_{,xx}$, $\epsilon_{yy} = -zw_{,yy}$ and $\gamma_{xy} = -2zw_{,xy}$.

Straight lines normal to the undeformed midsurface are assumed to remain straight *and normal* to the deformed midsurface. Thus transverse shear deformation is zero throughout the Kirchoff plate (although transverse shear *forces* remain present). Many practical plates can be approximated by Kirchoff plates, since they are thin enough for transverse shear deformation to be negligible.

The displacement field assumed in Equation (3.2) yields in-plane strains of the form

$$\epsilon_{xx} = z\theta_{x,x} = -zw_{,xx}, \quad \epsilon_{yy} = z\theta_{y,y} = -zw_{,yy}, \quad \gamma_{xy} = z(\theta_{x,y} + \theta_{y,x}) = -2zw_{,xy} \quad , \tag{3.53}$$

where $\theta_{x,x} = \partial\theta_x/\partial x$, etc. The transverse shear strains are obtained as

$$\gamma_{xz} = w_{,x} + \theta_x = 0 \, , \quad \gamma_{yz} = w_{,y} + \theta_y = 0 \quad . \tag{3.54}$$

For plane stress and linear isotropic elasticity the foregoing strain field again defines the

in-plane stresses as

$$\sigma_{xx} = \frac{E}{1-\nu^2}[\epsilon_{xx} + \nu\epsilon_{yy}] \tag{3.55}$$

$$\sigma_{yy} = \frac{E}{1-\nu^2}[\epsilon_{yy} + \nu\epsilon_{xx}] \tag{3.56}$$

$$\sigma_{xy} = \sigma_{yx} = G\gamma_{xy} \quad , \tag{3.57}$$

where E is Young's modulus, ν is Poisson's ratio and $G = E/2(1+\nu)$. There are no out-of-plane stresses.

Integrating the in-plane stresses, which vary linearly along the plate thickness, gives stress resultants of the form

$$M_{xx} = \int_{-t/2}^{t/2} \sigma_{xx} z \; dz \tag{3.58}$$

$$M_{yy} = \int_{-t/2}^{t/2} \sigma_{yy} z \; dz \tag{3.59}$$

$$M_{xy} = M_{yx} = \int_{-t/2}^{t/2} \sigma_{xy} z \; dz \quad . \tag{3.60}$$

Introducing matrix notation, the foregoing are written as

$$\boldsymbol{M} = [M_{xx} \;\; M_{yy} \;\; M_{xy}]^T \quad , \tag{3.61}$$

and the curvatures $\boldsymbol{\kappa}$ as

$$\boldsymbol{\kappa} = [\theta_{x,x} \;\; \theta_{y,y} \;\; \theta_{x,y} + \theta_{y,x}]^T \quad . \tag{3.62}$$

It again follows that the moment-curvature relation may be expressed as

$$\boldsymbol{M} = \boldsymbol{D}_b \boldsymbol{\kappa} \quad , \tag{3.63}$$

where

$$\boldsymbol{D}_b = \frac{Et^3}{12(1-\nu^2)} \begin{bmatrix} 1 & \nu & 0 \\ \nu & 1 & 0 \\ 0 & 0 & (1-\nu)/2 \end{bmatrix} \quad . \tag{3.64}$$

The total plate energy, based on potential energy for bending and shear, is written as

$$\Pi = \frac{1}{2}\int_\Omega \boldsymbol{\kappa}^T \boldsymbol{D}_b \boldsymbol{\kappa} \; d\Omega - \Pi_{ext} \quad , \tag{3.65}$$

where Π_{ext} is the potential energy of the applied loads. The thin plate Kirchhoff conditions of Equations (3.23) should be satisfied in the finite element interpolation. The interested reader is referred to plate bending by Cook [22].

Chapter 4

Topology optimization of plate-like structures

The problem of variable thickness plate design and the placement of stiffeners in such design problems have received special attention.

The design of variable thickness Kirchoff and Mindlin plates is, at first glance, just another sizing problem that seeks the optimal continuously varying thickness of the plate. The close connection with the 0-1 topology design is not entirely evident, but the cubic dependence of plate bending stiffness on the thickness of the plate implies that the optimal design prefers to achieve either of the bounds on the thickness, which in essence is a plate with integral stiffeners. This in turn implies non-existence of solutions, unless the gradient of the thickness function is constrained [23].

4.1 Square Kirchoff plates

In this section, topology optimization of shear rigid plates is illustrated. A flat square plate is supported along all four of its ends and a unit load is applied at the center.

The procedure for computing an optimal plate design is analogous to that described in Chapter 2 and the optimality criteria and sensitivity carry over *ad verbatim*, with strains and stresses interpreted as curvatures and moments respectively.

In Figures 4.1, 4.2, 4.3 and 4.4, the square plate is optimized for different volume fractions. The optimized topology is also sought for different support conditions, i.e. clamped, simply supported and just supported. (Just supported is even "softer" than simply supported.) Throughout, a value of Poisson's ratio of 0.3 is used. The figures clearly demonstrate the important effect of boundary conditions, and also volume fraction.

Figure 4.5 depicts the deformed geometry of the plate in Figure 4.2(a) which is clamped, for a volume fraction of 0.5. Apart from the center, where the load is applied, it can be observed that there is a concentration of strain energy in the middle of the supported edges, which is where material 'builds up' during the optimization process.

('Initial strain energy' indicates the strain energy density observed after only one iteration,

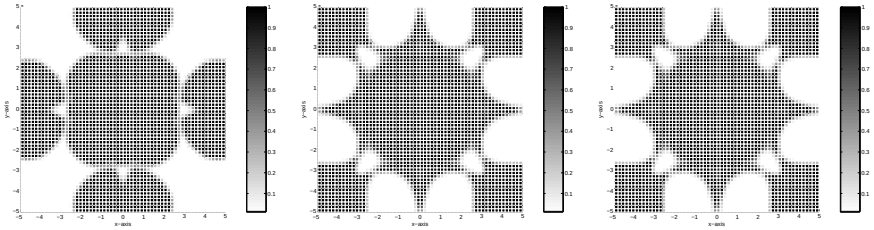

(a) *Clamped* (b) *Simply supported* (c) *Just supported*

Figure 4.1: Optimal shear rigid plates with a volume fraction of 0.625

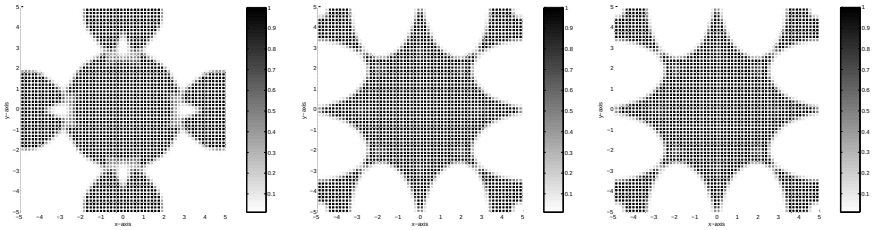

(a) *Clamped* (b) *Simply supported* (c) *Just supported*

Figure 4.2: Optimal shear rigid plates with a volume fraction of 0.5

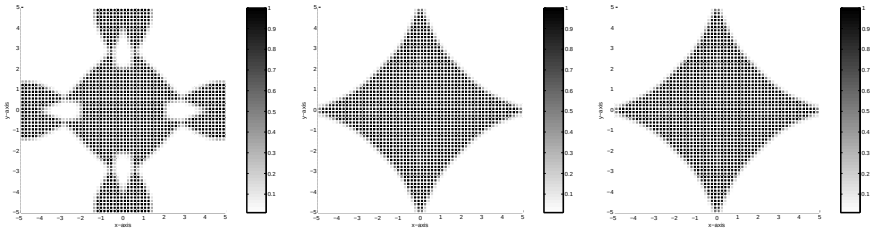

(a) *Clamped* (b) *Simply supported* (c) *Just supported*

Figure 4.3: Optimal shear rigid plates with a volume fraction of 0.375

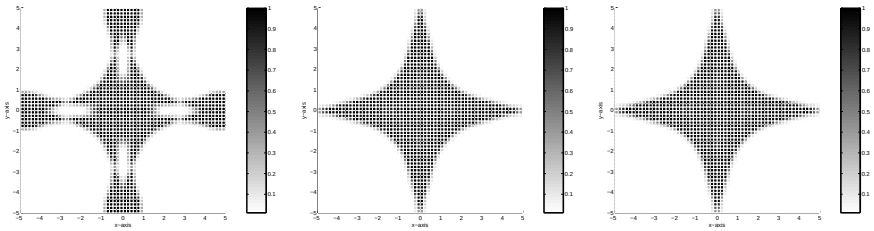

(a) *Clamped* (b) *Simply supported* (c) *Just supported*

Figure 4.4: Optimal shear rigid plates with a volume fraction of 0.25

when virtually no materials has been removed, with the initial densities all equal to 0.5.)

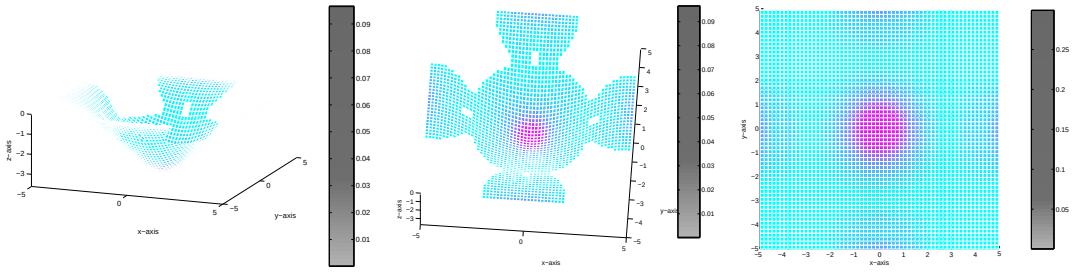

(a) *ISO view* (b) *Top view* (c) *Initial strain energy*

Figure 4.5: Optimal clamped shear rigid plate with a volume fraction of 0.5

Figure 4.6 depicts the deformed geometry of the plate in Figure 4.2(b) which is simply supported, with a volume fraction of 0.5. There is a high concentration of strain energy initially towards the corners, which results in some material accumulating in those areas. Since this model is shear rigid, no transverse shear deformation is allowed and nothing prevents the material from accumulating at the corners.

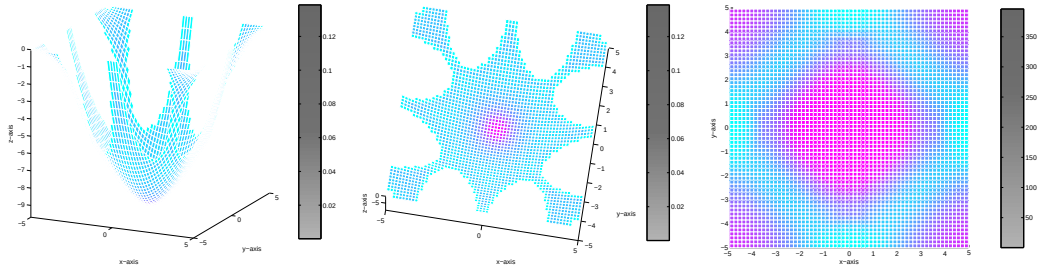

(a) *ISO view* (b) *Top view* (c) *Initial strain energy*

Figure 4.6: Optimal simply supported shear rigid plate with a volume fraction of 0.5

Figure 4.7 depicts the deformed geometry of the plate in Figure 4.2(c) which is just supported, with a volume fraction of 0.5. This case is very similar to the simply supported plate and the resulting topologies are similar, with the 'diagonal' material notable.

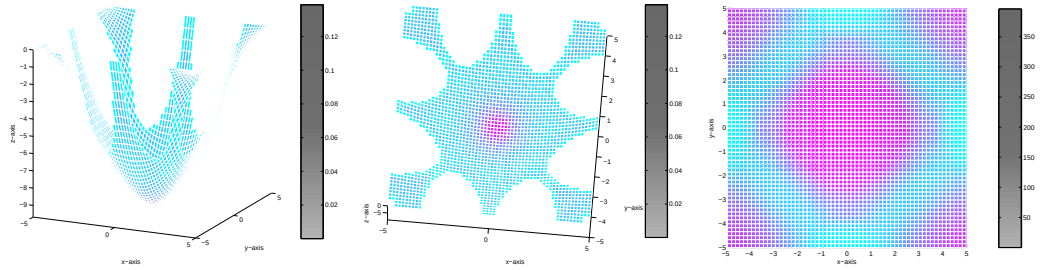

(a) *ISO view* (b) *Top view* (c) *Initial strain energy*

Figure 4.7: Optimal just supported shear rigid plate with a volume fraction of 0.5

4.1.1 Effect of Poisson's ratio

We now study the effect of Poisson's ratio on Kirchoff plates.

Figure 4.8 depicts the optimum topology for Poisson's ratio of 0.0; Figure 4.9 depicts the same for a Poisson's ratio of 0.49. For the simply supported and just supported the results differ dramatically.

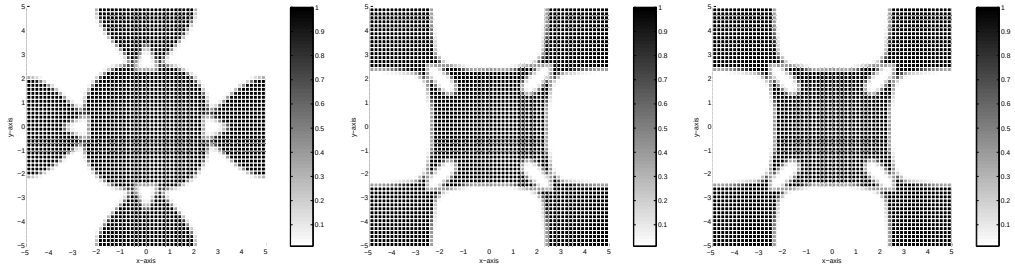

(a) *Clamped* (b) *Simply supported* (c) *Just supported*

Figure 4.8: Optimal shear rigid plates with a volume fraction of 0.5 and Poisson's ratio of 0.0

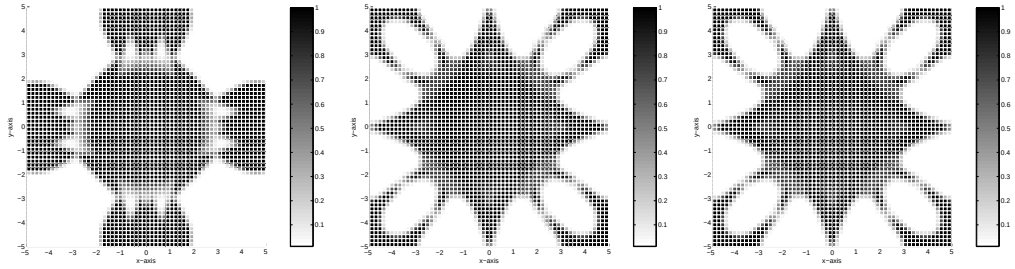

(a) *Clamped* (b) *Simply supported* (c) *Just supported*

Figure 4.9: Optimal shear rigid plates with a volume fraction of 0.5 and Poisson's ratio of 0.49

4.2 Square Mindlin plates

In this section, the topology optimization of shear flexible plates is now considered. As with the shear rigid plates, a flat square plate supported along all four of its ends, with a unit load applied to its center, is optimized.

In Figures 4.10, 4.11, 4.12 and 4.13, the plates are again optimized for different volume fractions. The optimized topology is also sought for different support conditions, i.e. clamped, simply supported and just supported. Again, the effects of boundary conditions and volume fraction are dramatic.

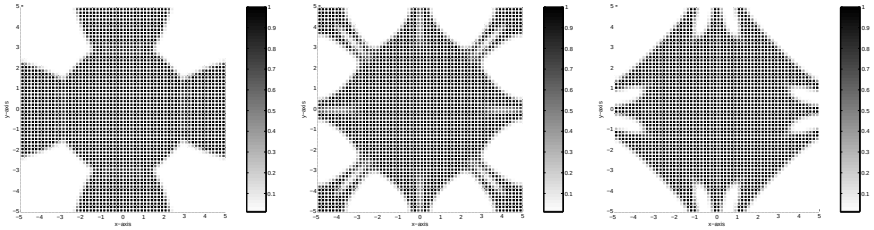

(a) *Clamped* (b) *Simply supported* (c) *Just supported*

Figure 4.10: Optimal shear flexible plates with a volume fraction of 0.625

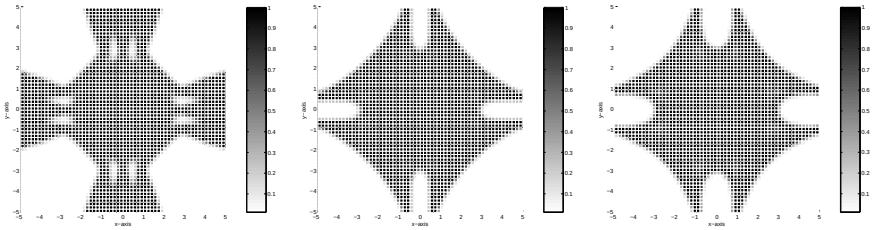

(a) *Clamped* (b) *Simply supported* (c) *Just supported*

Figure 4.11: Optimal shear flexible plates with a volume fraction of 0.5

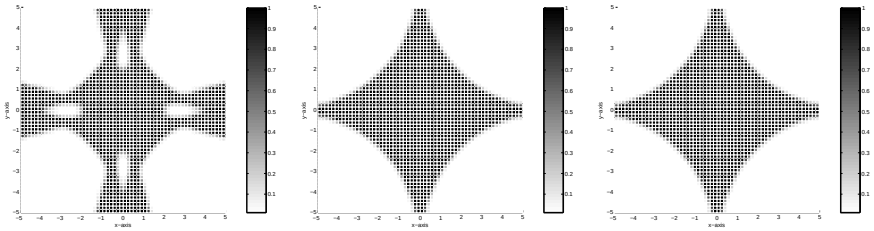

(a) *Clamped* (b) *Simply supported* (c) *Just supported*

Figure 4.12: Optimal shear flexible plates with a volume fraction of 0.375

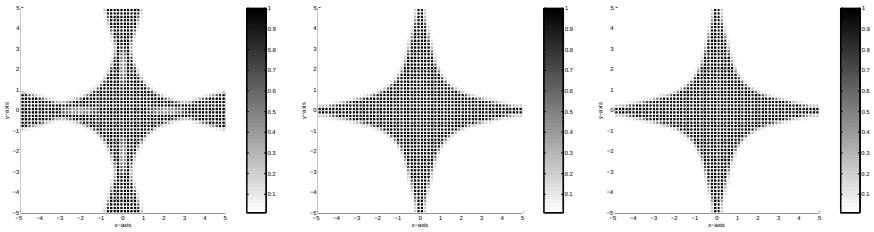

(a) *Clamped* (b) *Simply supported* (c) *Just supported*

Figure 4.13: Optimal shear flexible plates with a volume fraction of 0.25

Figure 4.14 depicts the deformed geometry of the plate in Figure 4.11(a) which is clamped, with a volume fraction of 0.5. It is again observed from the strain energy plot that there

is some strain energy concentrated in the middle of the supported edges; which is where material 'builds up' during the optimization process.

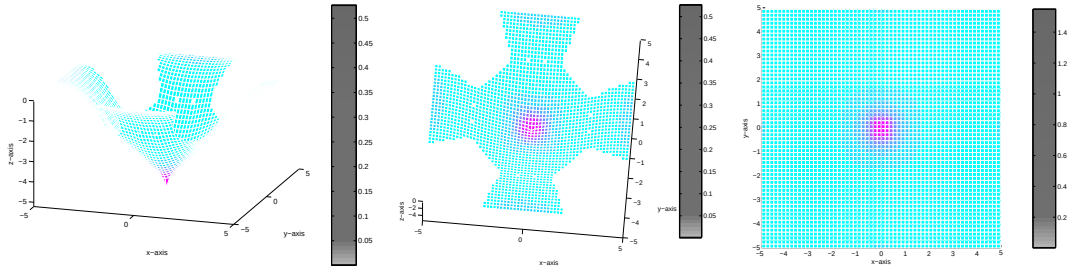

(a) *ISO view* (b) *Top view* (c) *Initial strain energy*

Figure 4.14: Optimal clamped shear flexible plate with a volume fraction of 0.5

Figure 4.15 depicts the deformed geometry of the plate in Figure 4.11(b) which is simply supported, with a volume fraction of 0.5. There is a high concentration of strain energy initially towards the corners, which results in material accumulating there. But unlike the shear rigid case, there is transverse shear deformation present, which seems to prevent the material from accumulating at the corners. The gap between the 'legs' in the middle of the plate edges seems testimony to the fact that the material would have moved towards the corners if transverse shear deformation was not allowed.

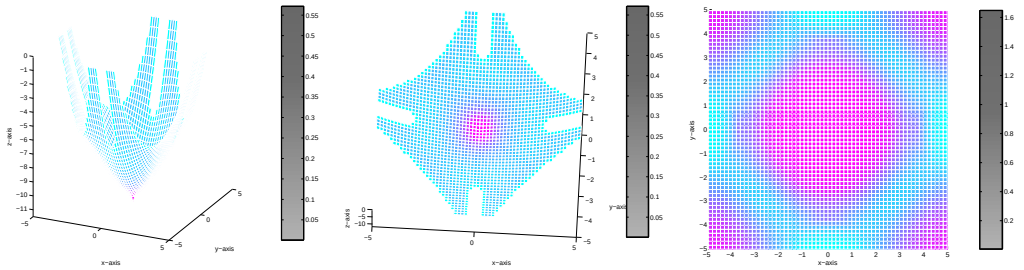

(a) *ISO view* (b) *Top view* (c) *Initial strain energy*

Figure 4.15: Optimal simply supported shear flexible plate with a volume fraction of 0.5

Figure 4.16 depicts the deformed geometry of the plate in Figure 4.11(c) which is just supported, with a volume fraction of 0.5. This case is similar to the simply supported plate and the resulting topologies are similar.

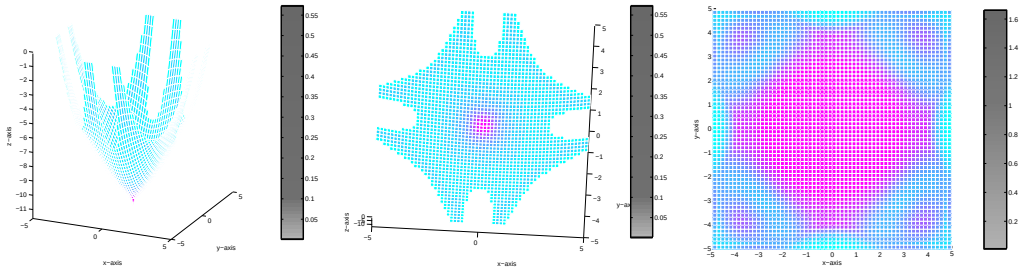

(a) *ISO view* (b) *Top view* (c) *Initial strain energy*

Figure 4.16: Optimal just supported shear flexible plate with a volume fraction of 0.5

4.2.1 Effect of Poisson's ratio

We now study the effect of Poisson's ratio on Mindlin plates.

Figure 4.17 depicts the optimum topology for Poisson's ratio of 0.0; Figure 4.18 depicts the same for a Poisson's ratio of 0.49. The differences are again dramatic, in particular for the simply supported case.

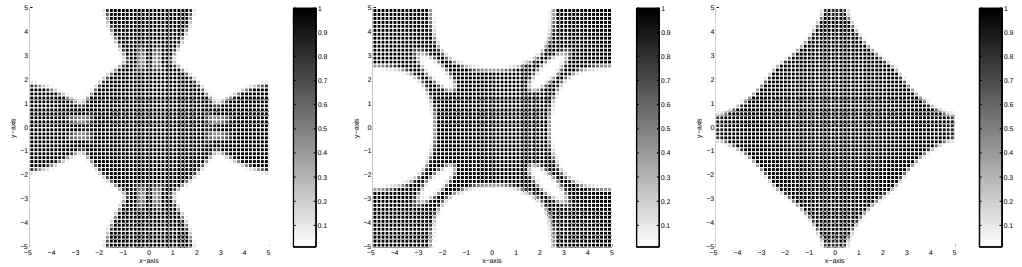

(a) *Clamped* (b) *Simply supported* (c) *Just supported*

Figure 4.17: Optimal shear flexible plates with a volume fraction of 0.5 and Poisson's ratio of 0.0

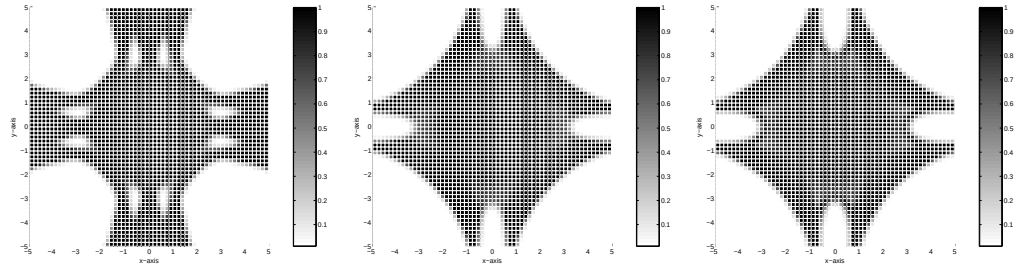

(a) *Clamped* (b) *Simply supported* (c) *Just supported*

Figure 4.18: Optimal shear flexible plates with a volume fraction of 0.5 and Poisson's ratio of 0.49

4.3 Closure

In this chapter, both shear flexible Mindlin plate elements and shear rigid Kirchoff plate elements were used to determine the optimal topologies of plates with different aspect ratios.

From the results tabulated in Appendix C, one can see that for the same parameters, shear flexible Mindlin plate elements yield better compliance values as compared to shear rigid Kirchoff plate elements. The results clearly illustrate the importance of through thickness shear. Qualitatively, the results obtained compare closely with some of the results obtained previously by Pedersen [24].

As expected, it can also be observed that clamped plates give better compliance values than the simply supported and just supported cases. The results obtained for the simply supported and just supported cases, however, are generally very similar in both topology and compliance.

For both shear flexible Mindlin plate elements and shear rigid Kirchoff plate elements, compliance increases with an increase in Poisson's ratio.

Chapter 5

Flat shell elements

5.1 Flat shell elements

Shells are amongst the most complex structures to analyze numerically. A number of shell theories exist, i.e. deep, shallow and flat shell theory, each of them associated with particular assumptions and difficulties. Theoretical results associated with deep and shallow theory may differ and the assumption of shallow theory in many instances can result in errors.

As noted by Bathe and Dvorkin [9, 13] the formulation of a finite element shell should not be based on a specific shell theory; it must be applicable to any plate or shell situation. Furthermore, the formulation should follow continuum mechanics theory as far as possible, while the assumptions made in finite element discretization should be mechanistically clear and well-founded. No spurious modes should be present, and the formulation must be totally free from locking.

Flat shell elements are easy to define geometrically and will always converge to the correct deep shell solution in the limit of mesh refinement.

Analytical through-thickness integration is easily performed for flat shells as the Jacobian $\boldsymbol{J}$ of the transformation is constant through the thickness. The flat shell elements with in plane degrees of freedom (d.o.f.) also allow for easy coupling with edge beam and rib members.

5.1.1 A general flat shell formulation

Without development, we assume that a membrane element with drilling d.o.f. is available [25]. We then continue this element with the elements proposed in Chapter 3, to form a flat shell element.

The element force-displacement relationship of a membrane element with in-plane drilling degrees of freedom is defined as

$$\boldsymbol{K}_m \boldsymbol{q}_m = \boldsymbol{f}_m \quad , \tag{5.1}$$

where $\boldsymbol{K}_m$ denotes the membrane stiffness matrix, $\boldsymbol{q}_m$ the element displacements and $\boldsymbol{f}_m$ the element loads.

The unknown nodal displacements $\boldsymbol{q}_m$ and the consistent nodal loads $\boldsymbol{f}_m$ are defined by

$$\boldsymbol{q}_m^i = [u_i \quad v_i \quad \theta_{zi}]^T \tag{5.2}$$

$$\boldsymbol{f}_m^i = [U_i \quad V_i \quad M_{zi}]^T \quad , \tag{5.3}$$

where θ_{zi} is the in-plane nodal rotation and M_{zi} the in-plane nodal moment.

Similarly, the Mindlin-Reissner plate element force-displacement relationship is written as

$$(\boldsymbol{K}_b + \bar{\boldsymbol{K}}_s)\boldsymbol{q}_p = \boldsymbol{f}_p \quad , \tag{5.4}$$

where $\boldsymbol{K}_b$ is the bending stiffness and $\bar{\boldsymbol{K}}_s$ the shear stiffness associated with the substitute assumed strain interpolation. Subscripts b, s and p indicate bending, shear and plate respectively. The displacements $\boldsymbol{q}_p$ and the consistent nodal loads $\boldsymbol{f}_p$ are respectively defined by

$$\boldsymbol{q}_p^i = [w_i \quad \theta_{xi} \quad \theta_{yi}]^T \tag{5.5}$$

$$\boldsymbol{f}_p^i = [W_i \quad M_{xi} \quad M_{yi}]^T \quad . \tag{5.6}$$

Employing matrix notation, the element stiffness matrix of a flat shell element is obtained in an element local coordinate system as

$$\boldsymbol{K} = \begin{bmatrix} \boldsymbol{K}_m & (\boldsymbol{K}_{mb} + \boldsymbol{K}_{ms}) \\ symm & (\boldsymbol{K}_b + \bar{\boldsymbol{K}}_s) \end{bmatrix} \quad . \tag{5.7}$$

Double subscripts imply coupling, e.g. subscript mb indicates coupling between in-plane membrane and out-of-plane bending actions.

It is normally assumed that coupling between transverse shear strains and in-plane membrane strains and bending strains respectively is absent, i.e.

$$\boldsymbol{K}_{ms} = \boldsymbol{K}_{bs} = 0 \quad . \tag{5.8}$$

This is not a necessary requirement for the formulation, but merely simplifies the presentation. Nevertheless, such coupling is rarely encountered in engineering practice.

On the other hand, coupling between membrane and bending actions ($\boldsymbol{K}_{mb}$) is extremely important when the reference surface is eccentric or if the material properties vary unsymmetrically with respect to the mid-surface.This includes coupling due to the hierarchical membrane bubble interpolation function (indicated by $\boldsymbol{K}_{bh}$). The expression for $\boldsymbol{K}$ presented in Equation 5.7 therefore reduces to

$$\boldsymbol{K} = \begin{bmatrix} \boldsymbol{K}_m & \boldsymbol{K}_{mb} \\ symm & (\boldsymbol{K}_b + \bar{\boldsymbol{K}}_s) \end{bmatrix} \quad . \tag{5.9}$$

However, for isotropic materials

$$\boldsymbol{K}_{mb} = 0 \quad . \tag{5.10}$$

The element stiffness matrix $\boldsymbol{K}$ therefore reduces to

$$\boldsymbol{K} = \begin{bmatrix} \boldsymbol{K}_m & 0 \\ symm & (\boldsymbol{K}_b + \bar{\boldsymbol{K}}_s) \end{bmatrix} \quad . \tag{5.11}$$

The local shell force-displacement relationship is given by

$$\boldsymbol{K}\boldsymbol{q} = \boldsymbol{f} \quad , \tag{5.12}$$

where the shell nodal displacements and loads respectively are

$$\boldsymbol{q}_i = [u_i \quad v_i \quad w_i \quad \theta_{xi} \quad \theta_{yi} \quad \theta_{zi}]^T \tag{5.13}$$

$$\boldsymbol{f}_i = [U_i \quad V_i \quad W_i \quad M_{xi} \quad M_{yi} \quad M_{zi}]^T \quad . \tag{5.14}$$

In Equations (5.7), (5.9) and (5.11), the partition stiffness matrices are given by

$$\boldsymbol{K}_m = \int_\Omega \boldsymbol{B}_m^T \boldsymbol{C}^m \boldsymbol{B}_m \quad \mathrm{d}\Omega \tag{5.15}$$

$$\boldsymbol{K}_b = \int_\Omega \boldsymbol{B}_b^T \boldsymbol{C}^b \boldsymbol{B}_b \quad \mathrm{d}\Omega \tag{5.16}$$

and

$$\bar{\boldsymbol{K}}_s = \int_\Omega \bar{\boldsymbol{B}}_s^T \boldsymbol{C}^s \bar{\boldsymbol{B}}_s \quad \mathrm{d}\Omega \quad . \tag{5.17}$$

Chapter 6

Topology optimization using flat shell elements

6.1 Introduction

In this chapter, an application of topology optimization using the flat shell elements presented in Chapter 5 is given. The Scordelis-Lo roof is selected as a test problem; it is depicted in Figure 6.1. (In Figure 6.1, the units are consistent.)

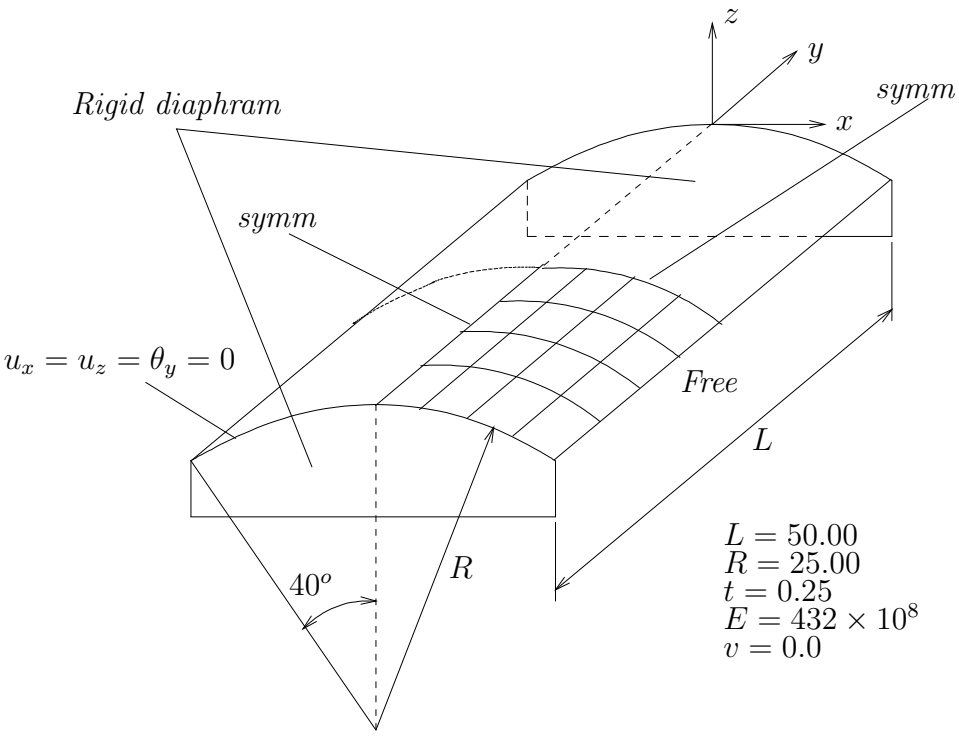

Figure 6.1: Scordelis-Lo Roof

6.2 Scordelis-Lo roof: geometry and characteristic

In the Scordelis-Lo roof, a downward point load (i.e. in the negative z direction) is applied to the geometric center of the roof. The Scordelis-Lo roof has an interesting characteristic in that a *downward* point load applied to its center causes the middle of its straight free edges to deflect *upward*.

The optimization is performed for one quarter of the roof, symmetry is used to depict the complete structure.

6.2.1 Scordelis-Lo roof results for a volume fraction of 0.5

Firstly, the Scordelis-Lo roof is optimized with a volume fraction of 0.5 and for different mesh discretizations, using MMA. The penalty parameter p is ramped up to a value of 5 over 167 iterations, whereafter it is kept constant for a further 83 iterations. Figure 6.2 depicts the optimal roof for a 4×4 mesh. (Again note that the reported discretizations are for a quarter of the roof only.)

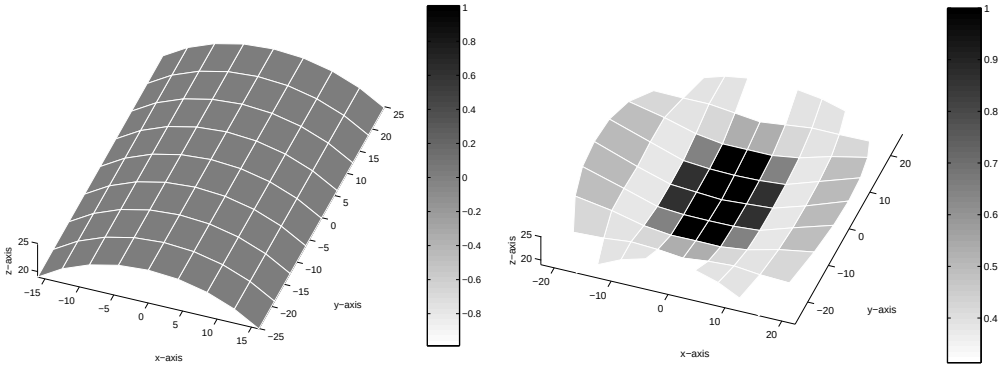

(a) *Original mesh* (b) *Optimized structure*

Figure 6.2: Scordelis-Lo roof (4×4 mesh, volume fraction of 0.5)

Figures 6.3, 6.4, 6.5 and Figure 6.6 respectively depict results for a 8×8, 16×16, 32×32 and a 64×64 mesh discretization.

The structure becomes more refined for finer mesh sizes. For coarse meshes, the structure appears to have large areas with intermediate densities.

On taking a closer look at the structures discretized using a 16×16, 32×32 and 64×64 mesh, as depicted in Figures 6.4(b), 6.5(b) and 6.6(b), one can see that more material accumulates at the load application point. The remainder of the material forms 'ribs' in a manner that optimally stiffens the structure.

The finer meshes, which yield better developed structures, also have lower compliance values, as can be observed from the objective function values tabulated in Table 6.1. The finer the discretization, the better the compliance (the stiffer the structure).

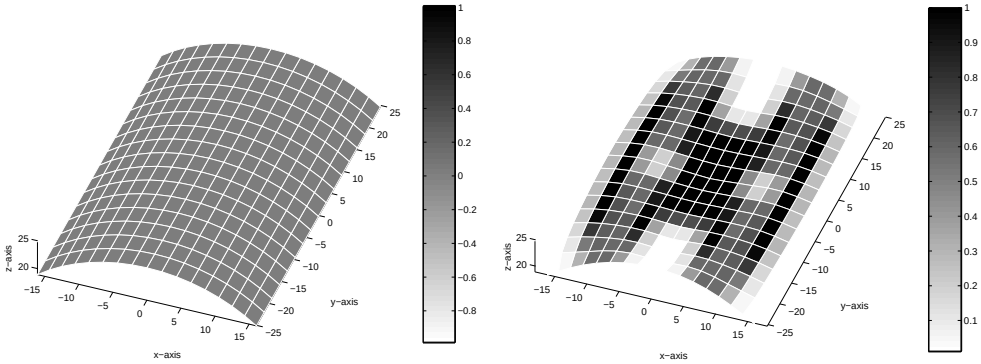

(a) *Original mesh* (b) *Optimized structure*

Figure 6.3: Scordelis-Lo roof (8×8 mesh, volume fraction of 0.5)

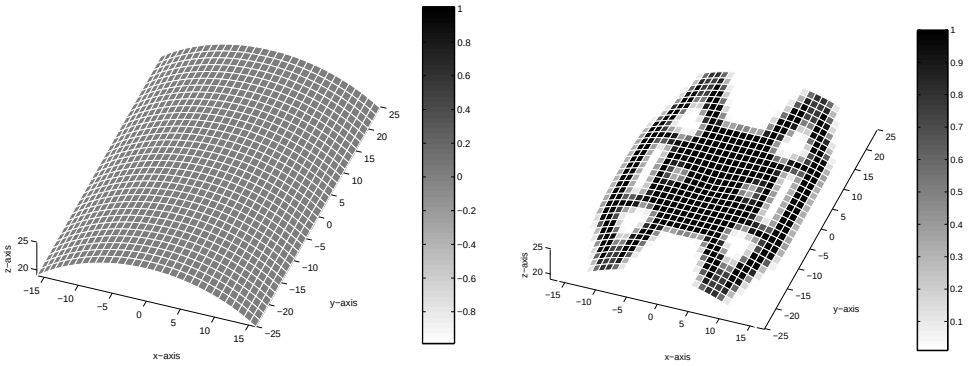

(a) *Original Mesh* (b) *Optimized structure*

Figure 6.4: Scordelis-Lo roof (16×16 mesh, volume fraction of 0.5)

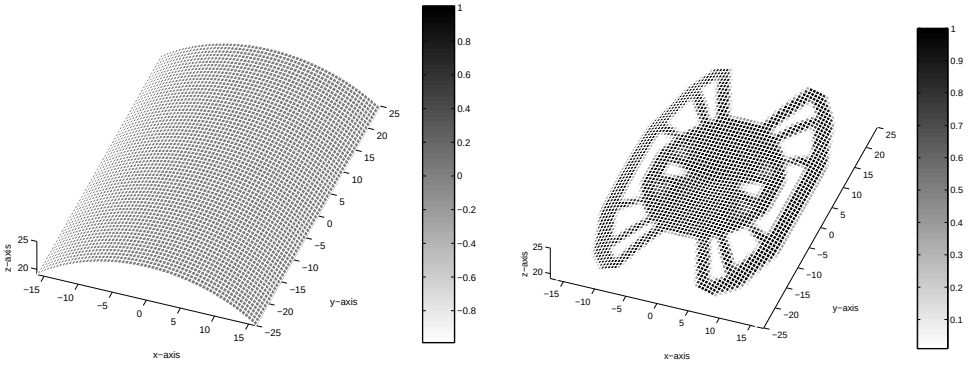

(a) *Original Mesh* (b) *Optimized structure*

Figure 6.5: Scordelis-Lo roof (32×32 mesh, volume fraction of 0.5)

To try to form a clearer understanding of how the structure behaves, several approaches are

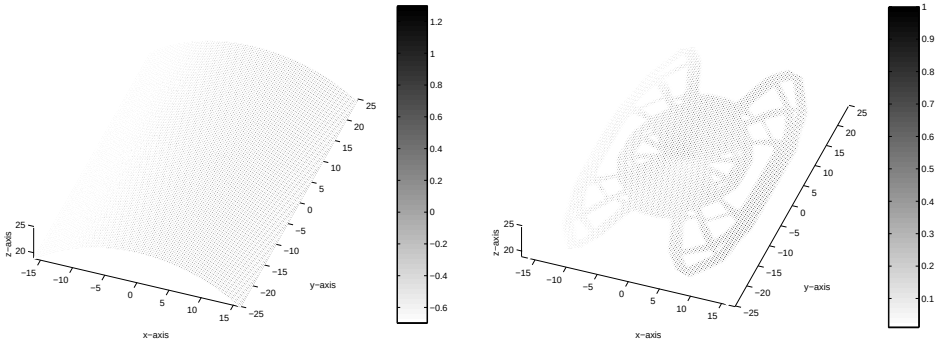

(a) *Original Mesh* (b) *Optimized structure*

Figure 6.6: Scordelis-Lo roof (64×64 mesh, volume fraction of 0.5)

Mesh size	Volume fraction	Objective function value
4×4	0.530	.492307E+06
8×8	0.500	.220180E+06
16×16	0.500	.147691E+06
32×32	0.500	.131398E+06
64×64	0.500	.124664E+06

Table 6.1: Scordelis-Lo roof results (penalty = 5, volume fraction = 0.5)

now followed. The structure is optimized for different volume fractions, namely 0.3, 0.5 and 0.7. It is also optimized with different penalty factors, namely 5 and (a very high value of) 9. The effect that stiffeners may have on the structure is also studied. The 32×32 mesh discretization is chosen for all further analyses.

6.2.2 Scordelis-Lo roof with different volume fractions and different penalty parameters

Scordelis-Lo roof with different volume fractions and a penalty of 5

The Scordelis-Lo roof is now optimized with different volume fractions. The penalty parameter is again ramped up to a value of 5 over 250 iterations.

The structures with the volume fractions of 0.3 and 0.5, depicted in Figures 6.7(a) and 6.7(b) respectively, are well defined, while the structure with a volume fraction of 0.7 depicted in Figure 6.7(c) looks a bit indistinct. The results are tabulated in Table 6.2, and as expected, compliance can be seen to improve with an increase in volume fraction.

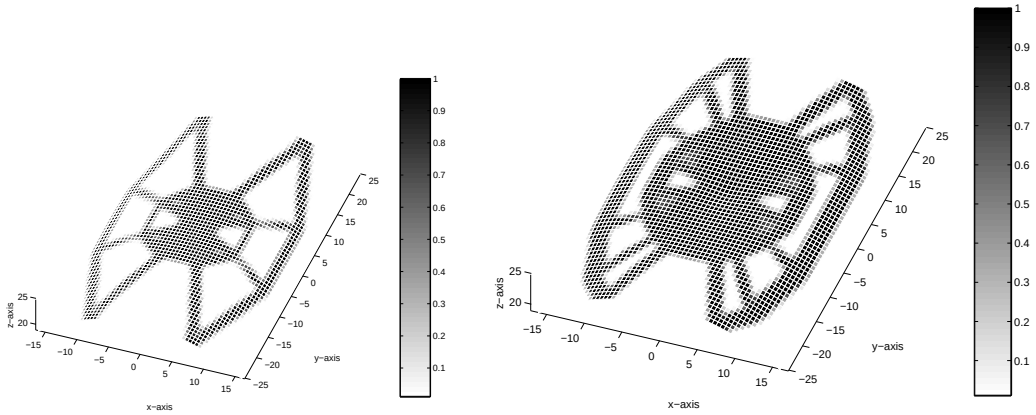

(a) *Volume fraction = 0.3*

(b) *Volume fraction = 0.5*

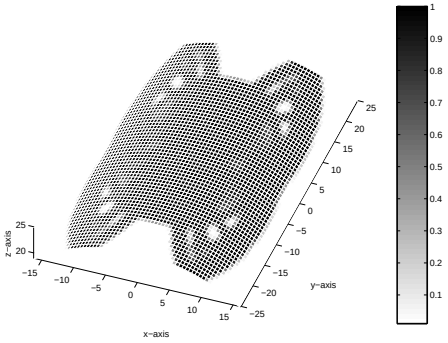

(c) *Volume fraction = 0.7*

Figure 6.7: Scordelis-Lo roof (32×32 mesh, penalty parameter of 5)

Volume fraction	Objective function value
0.300	.258162E+06
0.500	.131398E+06
0.700	.967719E+05

Table 6.2: Scordelis-Lo roof results with different volume fractions and a penalty parameter of 5

Scordelis-Lo roof with different volume fractions and a penalty of 9

The Scordelis-Lo roof is now again optimized for different volume fractions. The penalty parameter is however ramped up to a value of 9 over 250 iterations.

Results similar to those of the structure optimized with a penalty parameter value of 5 are obtained. The structures with volume fractions of 0.3 and 0.5, depicted in Figures 6.8(a) and 6.8(b) respectively, are better defined, while the structure with a volume fraction of 0.7 in Figure 6.8(c) still looks a bit indistinct. The results are tabulated in Table 6.3, and once again compliance can be seen to improve with an increase in volume fraction.

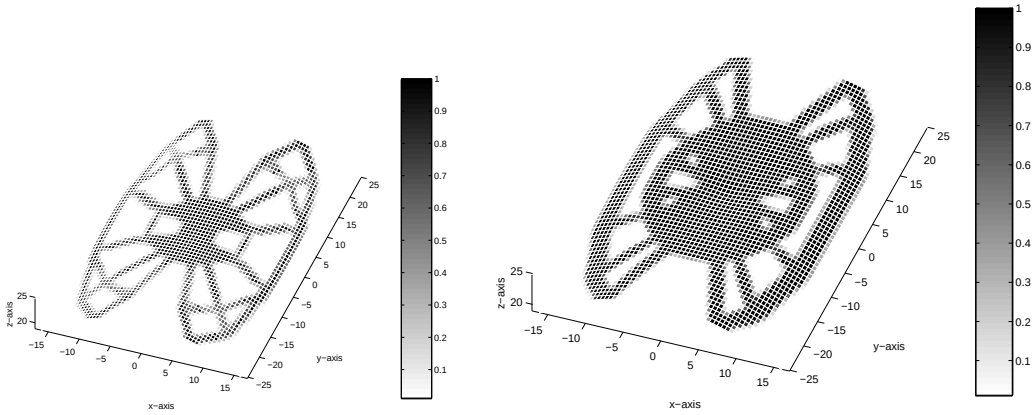

(a) *Volume fraction = 0.3*

(b) *Volume fraction = 0.5*

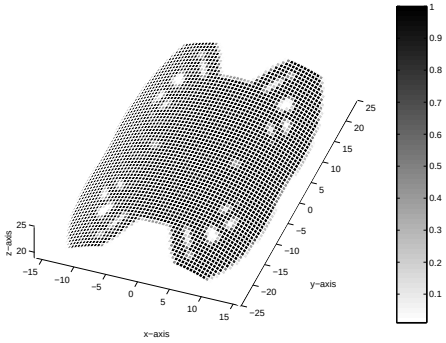

(c) *Volume fraction = 0.7*

Figure 6.8: Scordelis-Lo roof (32×32 mesh, penalty parameter of 9)

The use of very high penalty factors is in general not recommended, since this can easily lead to badly scaled stiffness matrices. The results in Tables 6.2 and 6.3 were obtained with a minimum density $x_{min} = 1 \times 10^{-2}$. For volume fractions of 0.5 and 0.7, this converged satisfactory. However, for the volume fraction of 0.3, there is a large discrepancy between the results obtained with a penalty of 5, and the results obtained with a penalty of 9 (see Tables 6.2 and 6.3 respectively). The results obtained with a penalty of 9 seems to be a local minimum. If the number of iterations for the penalty value of 9 is increased from 250 to 500, the final result compares closely with the result obtained with a penalty of 5 (not shown in tabulated form).

The higher penalty parameter yields a slightly better defined structure. Figure 6.8(a) has more ribs than Figure 6.7(a), and the holes in Figures 6.8(b) and 6.8(c) are more developed than those in Figures 6.7(b) and 6.7(c) respectively.

Volume fraction	Objective function value
0.300	.685575E+06
0.500	.134274E+06
0.700	.970547E+05

Table 6.3: Scordelis-Lo roof results with different volume fractions and a penalty parameter of 9

6.2.3 Scordelis-Lo roof with stiffeners

The effect of stiffeners on the optimal roof topology is now studied. Three predetermined positions for longitudinal stiffeners are considered (see Figure 6.9). The volume fraction of the structure, and the size and position of the stiffeners are varied. The inner stiffener is positioned at a quarter of the distance from the roofs center to the straight free edge (nearer to the center), the outer stiffener is positioned at three quarters of the distance from the roofs center to the straight free edge (nearer to the edge), and the middle stiffener is positioned halfway between the roofs center and the straight free edge. (Again see Figure 6.9.)

Two different stiffeners are considered: 'shallow' stiffeners with height equal to 4 times the shell thickness, and 'deep' stiffeners, 5 times higher than the shallow stiffeners.

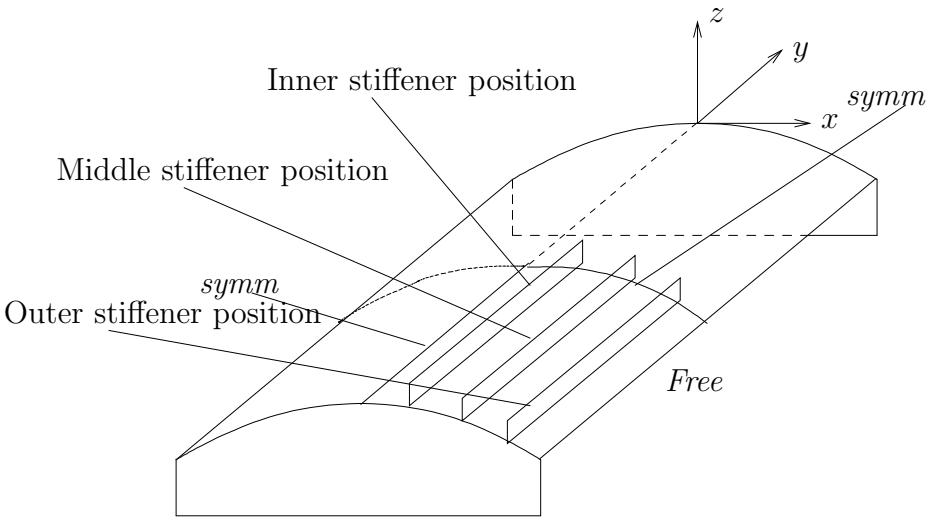

Figure 6.9: Scordelis-Lo Roof with stiffeners

Figure 6.10 depicts the shallow stiffeners placed on the structure with a volume fraction of 0.3. The numerical results are tabulated in Table 6.4.

Although the stiffeners appear to be nonexistent in Figures 6.10(a) and 6.10(b), they have altered the topology of the structure when compared to the one in Figure 6.7(a), and the compliance has a very small improvement. A more substantial improvement in compliance is realized where the outer stiffener is used; its different topology is depicted in Figure 6.10(c).

Figure 6.11 depicts the shallow stiffeners placed on the structure with a volume fraction of 0.5. The numerical results are shown in Table 6.5.

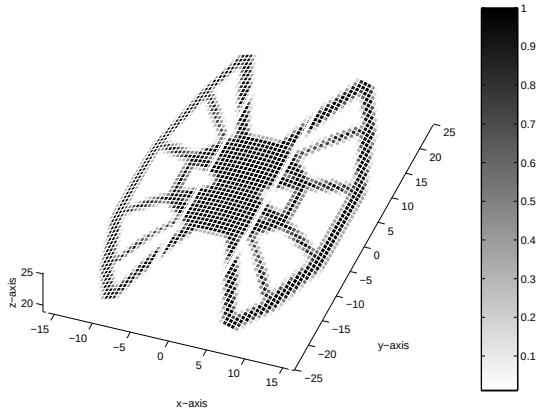

(a) *inner stiffener*

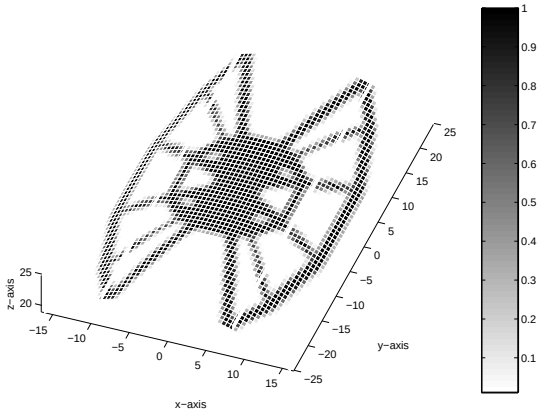

(b) *middle stiffener*

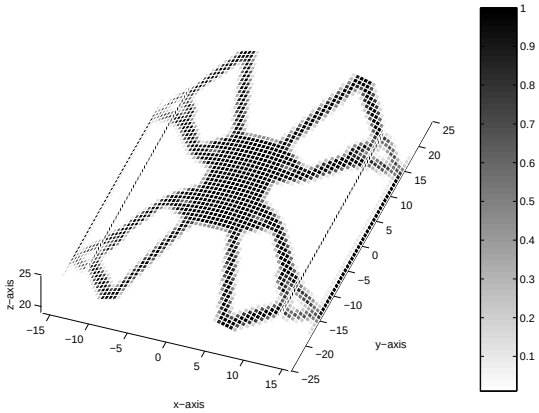

(c) *outer stiffener*

Figure 6.10: Scordelis-Lo roof with shallow stiffeners (32×32 mesh, volume fraction of 0.3)

Stiffener position	Objective function value
inner	.257165E+06
middle	.255939E+06
outer	.245373E+06

Table 6.4: Scordelis-Lo roof results with shallow stiffeners and a volume fraction of 0.3

The stiffeners in Figures 6.11(a) and 6.11(b) also appear to be nonexistent, and there is only a small improvement in compliance. Once again a more substantial improvement in compliance is realized where the outer stiffener is used and its existence is evident in Figure 6.11(c).

Figure 6.12 depicts the effect of the deep stiffeners on the structure, for a volume fraction of 0.5. The numerical results are shown in Table 6.6.

The deep stiffeners used in Figure 6.12(a), 6.12(b) and 6.12(c) all have an effect on the structure. They all give a huge improvement in compliance. The middle stiffener has the

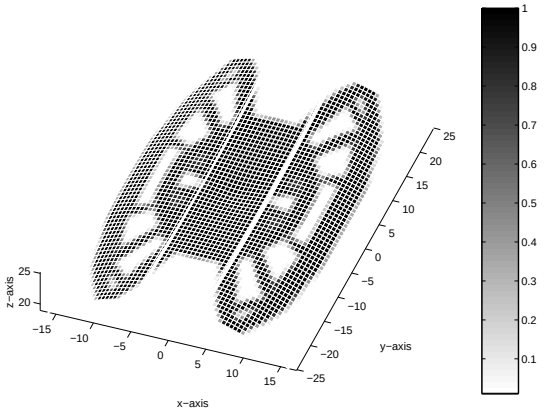

(a) *inner stiffener*

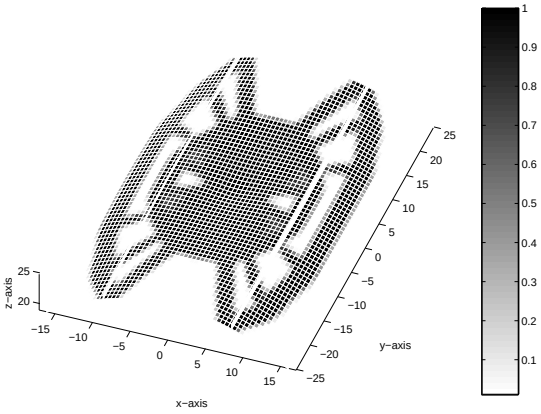

(b) *middle stiffener*

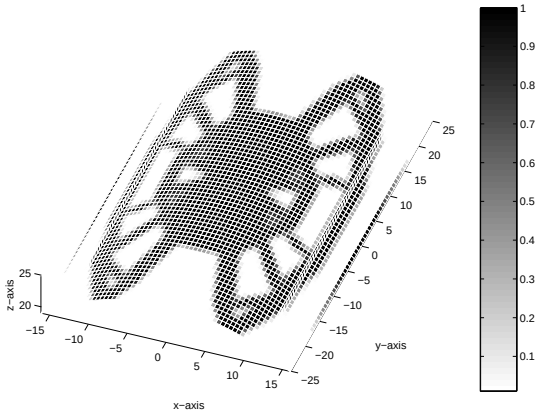

(c) *outer stiffener*

Figure 6.11: Scordelis-Lo roof with shallow stiffeners (32×32 mesh, volume fraction of 0.5)

Stiffener position	Objective function value
inner	.127393E+06
middle	.127498E+06
outer	.122766E+06

Table 6.5: Scordelis-Lo roof results with shallow stiffeners and a volume fraction of 0.5

least improvement, the outer stiffener a larger improvement, and the inner stiffener has the most dramatic effect on the topology of the structure; yielding the largest improvement.

The outer stiffener generally yields a larger improvement in compliance than the inner and the middle stiffener. The size of the stiffener also has a very big effect on the structure (the deeper the stiffener, the bigger its effect is on improving the structures compliance). The stiffeners generally yield a different topology to that of a structure without stiffeners.

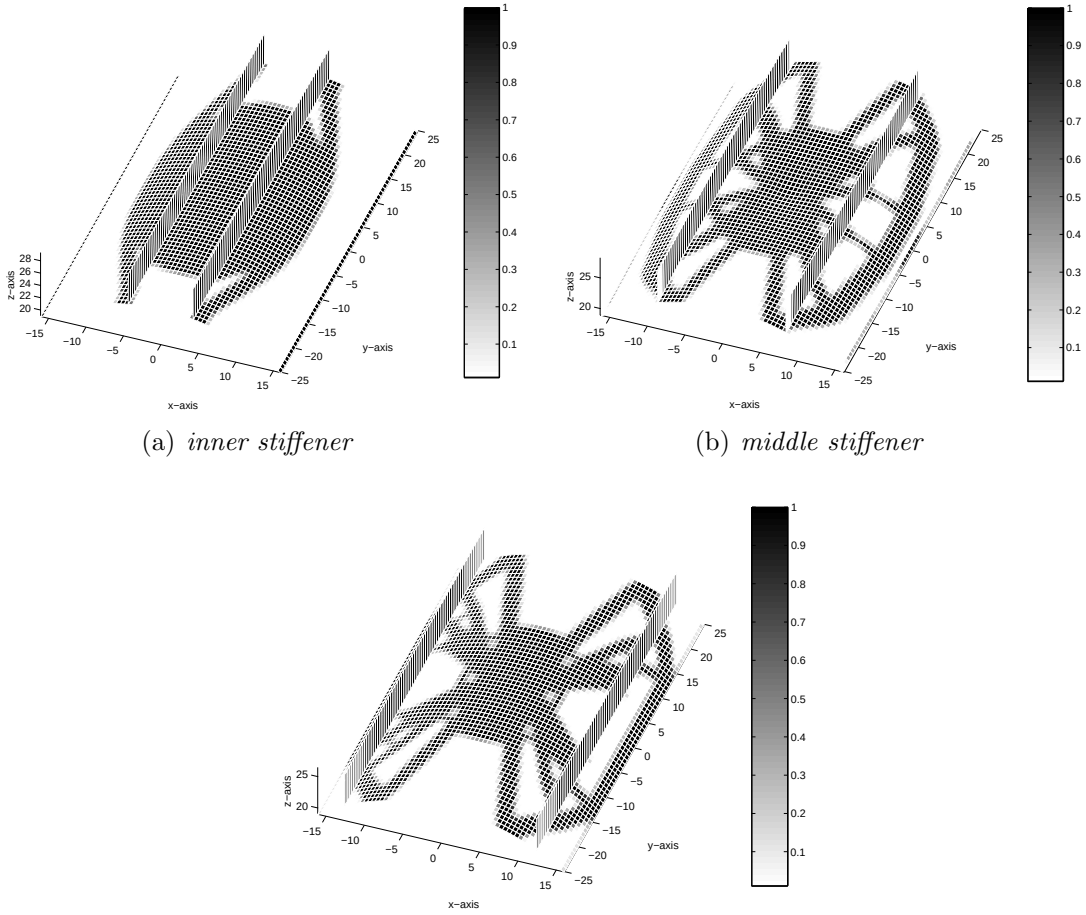

(a) *inner stiffener*

(b) *middle stiffener*

(c) *outer stiffener*

Figure 6.12: Scordelis-Lo roof with deep stiffeners (32×32 mesh, volume fraction of 0.5)

Stiffener position	Objective function value
inner	.658966E+05
middle	.122950E+06
outer	.985164E+05

Table 6.6: Scordelis-Lo roof results with deep stiffeners and a volume fraction of 0.5

6.3 Plate with the Scordelis-Lo roof's aspect ratio

A plate with an aspect ratio of the roof is now also optimized in an attempt to get some clarity on the results obtained for the roof structure, and to assess the effect of curvature.

The plate is constrained in the same manner as the roof, with the long edges being free and a point load applied at the center. The stiffeners are positioned midway between the center of the plate and the free edges.

Figure 6.13 depicts the topology of a plate with a 32×32 mesh discretization, a penalty parameter of 5 and a volume fraction of 0.3, while Figure 6.14 depicts the topology of a plate with a 32×32 mesh discretization, a penalty parameter of 5, but a volume fraction of 0.5.

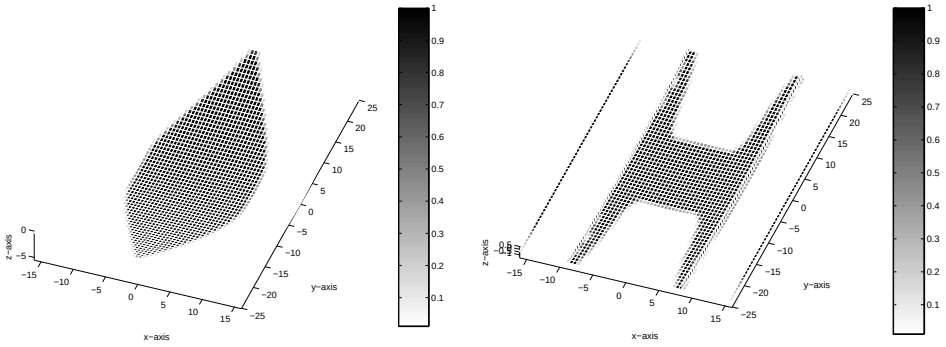

(a) *without stiffener* (b) *with stiffener*

Figure 6.13: Plate with the roof's aspect ratio (32×32 mesh, volume fraction of 0.3)

Stiffener	Objective function value
without stiffener	.132426E+08
with stiffener	.329770E+07

Table 6.7: Plate results with and a volume fraction of 0.3

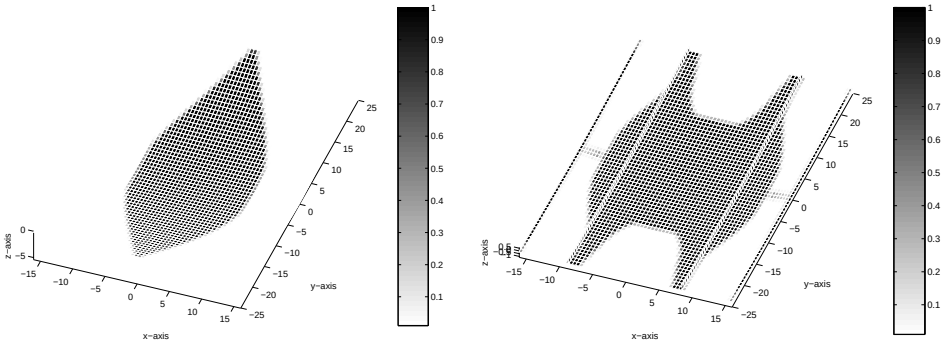

(a) *without stiffener* (b) *with stiffener*

Figure 6.14: Plate with the roof's aspect ratio (32×32 mesh, volume fraction of 0.5)

The numerical results to Figure 6.13 and Figure 6.14 are shown in Table 6.7 and Table 6.8 respectively. In both cases, the stiffener improves the compliance quite significantly; it is fully utilized.

Stiffener	Objective function value
without stiffener	.910575E+07
with stiffener	.259044E+07

Table 6.8: Plate results with and a volume fraction of 0.5

Chapter 7

Conclusions

7.1 General remarks

The objective of the study has been accomplished, that is, the topology optimization of a shell structure was successfully performed.

In doing so, both shear flexible Mindlin plate elements and shear rigid Kirchoff plate elements were used in determining the optimal topologies of plates with different aspect ratios. The results obtained compare closely with some of the results obtained previously by Pedersen.

Flat shell elements were then constructed, by combining the plate elements with a membrane element. These elements were then used in the optimization of the so-called Scordelis-Lo roof, and also a flat plate with the same aspect ratio as the roof. For the roof, material accumulates at the load application point; the remainder of the material forms ribs in a manner that optimally seeks to stiffen the structure.

A significant advantage of flat shell elements with drilling degrees of freedom is that the shells in a finite element model do not have to be co-planar, i.e. they can be joined at arbitrary angles, e.g. when modeling stiffeners.

In general, to improve the resolution of results in topology optimization, one needs to use finer meshes, and use a higher penalty factor (without introducing numerical instabilities). The mesh need not be finer than the resolution that is practically realizable. (The manufacturing of parts may prove very difficult, if not impossible, when many fine ribs or other detail is present.)

From an implementation point of view, it is noted that there is not a unique solution to a topology optimization problem. The solution obtained will be dependent on a number of factors, such as move limits, mesh discretization, penalty factor, filter type, etc. Even the algorithm or method used to solve the problem may yield different results for a given topology optimization problem.

Other modeling difficulties relate to the representation of loads and boundary constraints; different boundary conditions will yield different solutions, and it is not always clear how real boundary conditions can be represented mathematically. Hence special consideration should be given to the proper or realistic constraining of models.

7.2 Recommendations for future work

This preliminary study into the feasibility of using topology optimization to design shell structures approximated as flat facets proved successful. Nevertheless, further work will be beneficial.

A study of the *correlation* between the optimal results predicted in this thesis, and the behavior of a real structure in the laboratory, would be very interesting. This is suggested for some of the plate topologies generated, and also the Scordelis-Lo roof. (The singly curved geometry of this shell will probably be easier to manufacture than doubly curved shells.)

This study should also be furthered by topology optimization of structures with non-homogeneous materials. (This is probably also of interest in MEMS.)

The implementation of topology optimization of plates with 'passive elements', (i.e. prescribed holes or solid areas), and compliant mechanisms also seems interesting.

Another interesting aspect would be to explore the use of reliability based topology optimization (RBTO). RBTO may help in attaining a strong, but also reliable structure.

Finally, it seems desirable to implement stress constraints into the topology design problem considered.

Bibliography

[1] J. Stegmann and E. Lund. Nonlinear topology optimization of layered shell structures. *Struct. Multidisc. Opt.*, 29:349–360, 2005.

[2] S.A. Falco, S.M.B. Afonso, and L.E. Vaz. Analysis and optimal design of plates and shells under dynamic loads - i: finite element and sensitivity analysis. *Struct. Multidisc. Opt.*, 27:189–196, 2004.

[3] S.A. Falco, S.M.B. Afonso, and L.E. Vaz. Analysis and optimal design of plates and shells under dynamic loads - ii: optimization. *Struct. Multidisc. Opt.*, 27:196–209, 2004.

[4] M. Raulli and K. Maute. Topology optimization of electrostatically actuated microsystems. *Struct. Multidisc. Opt.*, 30:342–359, 2005.

[5] C.B.W. Pedersen and T. Buhl. Topology optimization. Notes placed on the internet, 2004.

[6] O. Sigmund. A 99 line topology optimization code written in matlab. *Struct. Multidisc. Opt.*, 21:120–127, 2001.

[7] K. Svanberg. MMA and some modelling aspects. In *Optimization systems and theory, KTH*, May 1999.

[8] T.A. Poulsen. A simple scheme to prevent checkerboard patterns and one-node connected hinges in topology optimization. *Struct. Multidisc. Opt.*, 24:396–399, 2002.

[9] K.-J. Bathe and E.N. Dvorkin. A four node plate bending element based on Mindlin-Reissner plate theory and a mixed interpolation. *Int. J. Numer. Methods Eng.*, 21:367–383, 1985.

[10] S. Ahmad, B.M. Irons, and O.C. Zienkiewicz. Analysis of thick and thin shell structures by curved finite elements. *Comp. Struct.*, 27:393–398, 1970.

[11] T. Belytschko and E. Bachrach. Efficient implementation of quadrilaterals with high coarse-mesh accuracy. *Comp. Meth. Applied Mech. Eng.*, 54:279–301, 1986.

[12] T. Belytschko and B.E. Engelman. Analysis of thick and thin shell structures by curved finite elements. *Comp. Struct.*, 25:909–918, 1987.

[13] E.N. Dvorkin and K.-J. Bathe. A continuum mechanics based four-node shell element for general non-linear analysis. *Eng. Comput.*, 1:77–88, 1984.

[14] E. Hinton and H.C. Huang. Shear forces and twisting moments in plates using Mindlin elements. *Eng. Comput.*, 3:129–142, 1986.

[15] P. Papadopoulos and R.L. Taylor. A triangular element based on Reissner-Mindlin plate theory. *Int. J. Numer. Methods Eng.*, 30:1029–1049, 1990.

[16] K.-J. Bathe. *Finite element procedures in engineering analysis*. Prentice-Hall, 1982.

[17] O.C. Zienkiewicz and R.L. Taylor. *The Finite Element method: Basic formulation and linear problems*, volume Vol II. McGraw-Hill, London, 1991.

[18] T.J.R. Hughes. *The finite element method: Linear static and dynamic analysis*. Series on Applied Mathematics. Prentice-Hall, Englewood Cliffs, New York, 1987.

[19] O.C. Zienkiewicz and R.L. Taylor. *The Finite Element method: Basic formulation and linear problems*, volume Vol I. McGraw-Hill, London, 1989.

[20] E.L. Wilson. The static condensation algorithm. *Int. J. Num. Meth. Eng.*, 8:199–203, 1974.

[21] H. Kebari. A one point integrated assumed strain 4-node Mindlin plate element. *Eng. Comput.*, 7:284–290, 1990.

[22] R.D. Cook. *Concepts and Applications of Finite Element Analysis*. Wiley, New York, 2002.

[23] M.P. Bendsoe and O. Sigmund. *Topology optimization: Theory, methods and applications*. Springer, Lyngby, Denmark, 2002.

[24] N.L. Pedersen. On topology optimization of plates with prestress. *International Journal of Numerical Methods in Engineering*, 51(2):225–240, 2001.

[25] S. Geyer and A.A. Groenwold. Two hybrid stress membrane finite element families with drilling rotations. *Int. J. Num. Meth. Eng.*, 53:583–601, 2002.

Appendix A

Filters

The difference between the filters is explained using a graphical means. In the presented figures, the filters are applied to the center element.

In Figure A.1 is a graphical illustration of a case where *no filter* is applied.

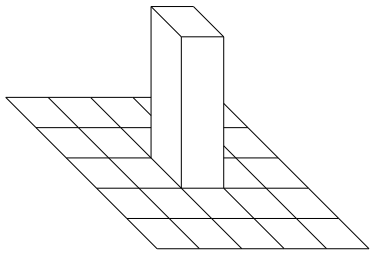

Figure A.1: No filter

A graphical illustration of a *linear filter* applied to the center element is shown in Figure A.2

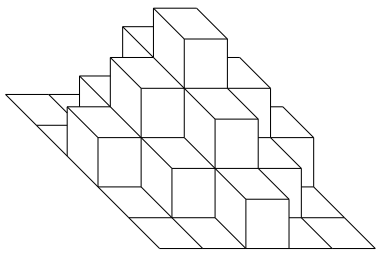

Figure A.2: Linear filter

Figure A.3 gives a graphical illustration of a *non-linear filter* applied to the center element.

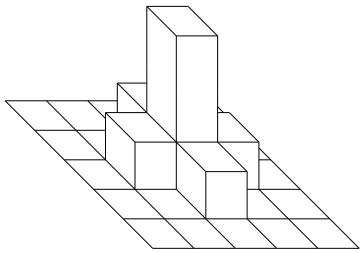

Figure A.3: Non-linear filter

A *3-by-3 filter* is described by

$$H = \frac{1}{(b+2)^2}\begin{bmatrix} 1 & b & 1 \\ b & b^2 & b \\ 1 & b & 1 \end{bmatrix} \quad b \in [1;\infty] \tag{A.1}$$

as explained in Section 2.3.

Appendix B

Descriptor function sensitivities

The local function h is defined as

$$h(a,b,c,d) = m(a,b,d).m(a,c,d).m(b,a,c).m(b,d,c) \tag{B.1}$$

The function m has the following symmetry

$$m(a,b,c) = m(c,b,a) \tag{B.2}$$

Then

$$\begin{array}{l} h(a,b,c,d) = \\ m_{,1}(a,b,d).m(a,c,d).m(b,a,c).m(b,d,c) + \\ m_{,1}(a,c,d).m(a,b,d).m(b,a,c).m(b,d,c) + \\ m_{,2}(b,a,c).m(a,b,d).m(a,c,d).m(b,d,c) \end{array} \tag{B.3}$$

where $h_{,k}$ denotes partial derivative with respect to the k^{th} entry. We note the m is not everywhere smooth, so we need to replace the absolute value by a smooth substitute. Numerical experiments show that replacing

$$|x| \quad \text{by} \quad A(x) = \sqrt{x^2 + \epsilon^2} - \epsilon \quad \text{with} \quad \epsilon = 0.1 \tag{B.4}$$

works well.

It is easy to check (using symmetry) that

$$h_{,2}(a,b,c,d) = h_{,1}(b,a,d,c) \tag{B.5}$$

$$h_{,3}(a,b,c,d) = h_{,1}(c,a,d,b) \tag{B.6}$$

$$h_{,4}(a,b,c,d) = h_{,1}(d,b,c,a) \tag{B.7}$$

Finally, we can write the sensitivity of the descriptor function as

$$\frac{dH}{de_{ij}}(\rho) = \sum_{ii=max(i-1,1)}^{min(i,n-1)} \sum_{jj=max(j-1,1)}^{min(j,m-1)} h_{,k}(d_{iijj}, d_{ii+1jj}, d_{iiij+1}, d_{ii+1ij+1}) \tag{B.8}$$

where $k = i - ii + 2(j - jj) + 1$.

Appendix C

Selected tabulated results

C.1 Square Kirchoff plate results

Support condition	Volume fraction	Objective function value
clamped	0.25	5953.743397
simply supported	0.25	.202515E+05
just supported	0.25	.202516E+05

Table C.1: Square Kirchoff plate results (penalty = 3, volume fraction = 0.25)

Support condition	Volume fraction	Objective function value
clamped	0.375	.373979E+04
simply supported	0.375	.114822E+05
just supported	0.375	.114823E+05

Table C.2: Square Kirchoff plate results (penalty = 3, volume fraction = 0.375)

Support condition	Volume fraction	Objective function value
clamped	0.50	2992.265149
simply supported	0.50	8061.084409
just supported	0.50	8061.109197

Table C.3: Square Kirchoff plate results (penalty = 3, volume fraction = 0.5)

Support condition	Volume fraction	Objective function value
clamped	0.625	.263720E+04
simply supported	0.625	.636679E+04
just supported	0.625	.636680E+04

Table C.4: Square Kirchoff plate results (penalty = 3, volume fraction = 0.625)

Support condition	Volume fraction	Objective function value
clamped	0.50	.349989E+04
simply supported	0.50	.867053E+04
just supported	0.50	.867053E+04

Table C.5: Square Kirchoff plate results (Poisson's ratio = 0, penalty = 3, volume fraction = 0.5)

Support condition	Volume fraction	Objective function value
clamped	0.50	.245261E+04
simply supported	0.50	.719621E+04
just supported	0.50	.719631E+04

Table C.6: Square Kirchoff plate results (Poisson's ratio = 0.49, penalty = 3, volume fraction = 0.5)

C.2 Square Mindlin plate results

Support condition	Volume fraction	Objective function value
clamped	0.25	.831921E+01
simply supported	0.25	.230059E+02
just supported	0.25	.230032E+02

Table C.7: Square Mindlin plate results (penalty = 3, volume fraction = 0.25)

Support condition	Volume fraction	Objective function value
clamped	0.375	.538545E+01
simply supported	0.375	.134928E+02
just supported	0.375	.134921E+02

Table C.8: Square Mindlin plate results (penalty = 3, volume fraction = 0.375)

Support condition	Volume fraction	Objective function value
clamped	0.50	4.326248
simply supported	0.50	9.558826
just supported	0.50	9.662013

Table C.9: Square Mindlin plate results (penalty = 3, volume fraction = 0.5)

Support condition	Volume fraction	Objective function value
clamped	0.624	.379768E+01
simply supported	0.625	.808107E+01
just supported	0.625	.780942E+01

Table C.10: Square Mindlin plate results (penalty = 3, volume fraction = 0.625)

Support condition	Volume fraction	Objective function value
clamped	0.50	.456208E+01
simply supported	0.50	.109974E+02
just supported	0.50	.112986E+02

Table C.11: Square Mindlin plate results (Poisson's ratio = 0, penalty = 3, volume fraction = 0.5)

Support condition	Volume fraction	Objective function value
clamped	0.50	.397463E+01
simply supported	0.50	.837988E+01
just supported	0.50	.838924E+01

Table C.12: Square Mindlin plate results (Poisson's ratio = 0.49, penalty = 3, volume fraction = 0.5)

Appendix D

Source code fragment

D.1 Notes

The code below is a modification of the 99-line matlab code developed by Sigmund [6]; it is based on the optimality criterion.

```
      program topo
c-----------------------------------------------------------------------c
      IMPLICIT REAL*8 (A-H,O-Z)
      CHARACTER*1 FIN*12,TITLE*1
      COMMON /PARC/ FIN,TITLE(80)
      COMMON /IOLIST/ NTM,NTR,NIN,NOT,NSP,NFL,NT7,NT8
      COMMON /TPRINT/ IPRINT
      DATA IPRINT /11/
c --- begin user input --- c
c      DATA FIN /'mbb'/
c      DATA FIN /'ptwist'/
c      DATA FIN /'fplt'/
      DATA FIN /'sclo32s'/
      PARAMETER (NXT=10000,NU1=40000,NU2=6,NU3=10) ! EL, NODES, DOF, LC
      PARAMETER (ND=24)                            ! DIM OF STIFFNESS MAT
c --- end user input --- c
      REAL*8 X(NXT)
      REAL*8 XOLD(NXT)
      REAL*8 XFEM(NXT)
      REAL*8 dc(NXT)
      REAL*8 dcold(NXT)
      REAL*8 U(NU1,NU2,NU3)
      REAL*8 S(NXT,NU2,NU3)
      REAL*8 E(ND,ND)
      REAL*8 Ue(ND)
      REAL*8 XYZ(3,4) ! COORDINATE, NODE NUMBER (1 .. 4)
c --- matlab pointers --- c
      integer engOpen,engClose,engEvalString
c-----------------------------------------------------------------------c
c --- open Matlab Session --- c
```

```
c      write(*,*) '--- opening matlab '
c      iep = engOpen('matlab ')
c      if (iep .eq. 0) then
c         write(6,*) 'Can''t start MATLAB engine'
c         stop
c      endif
c      write(*,*) '--- opening matlab complete '
c-----------------------------------------------------------------------c
c --- begin user input --- c
      nelx = 1*33
      nely = 1*32
      penalinit = 1.d0
      penalfinl = 5.d0
      volfrac=0.3d0
      rmin = 1.5d0
      maxit = 150
      chmax = 1.d0
c --- end user input --- c
c
      nel_tot = nelx*nely
      nnode_tot = (nelx+1)*(nely+1)
c
C --- CALL GRID GENERATION ROUTINE --- C
c      call gridgen_mbb(nelx,nely)
c      call gridgen_ptwist(nelx,nely)
c      call gridgen_fplt(nelx,nely)

c
c --- initialize densities --- c
      DO 10 I=1,nel_tot
        X(I) = volfrac
 10   CONTINUE
c
C ------------------ START OPTIMIXATION LOOP ------------------ C
c
      do 1234, iloop=0,maxit
c
c --- check for stopping criteria --- c
c      if (iloop.gt.maxit) then
c         goto 1234
c      elseif (chmax.lt.1.d-2) then
c         goto 1234
c      else
c         continue
c      endif
c
c --- ramp penalty term -- c
      fullpen=(2.d0/3.d0)*dble(maxit); ! number of iterations until penal=full
      penal=((penalfinl-penalinit)/fullpen)*dble(iloop) + penalinit;
      if (penal.gt.penalfinl)  penal=penalfinl
c
c --- open files for writing --- c
      open (file='disp.out',unit=50,status='unknown')
      open (file='nodes.out',unit=51,status='unknown')
```

```
      open (file='plotent.out',unit=52,status='unknown')
c
c --- calculate X for fem --- c
      DO 222 I=1,nel_tot
        XFEM(I) = X(I)**penal
 222  CONTINUE
c --- CALL EDSAP --- c
c
      CALL EDSAP(XFEM,NXT,U,NU1,NU2,NU3,MAXN,MAXL,NELEM,S)
c --- write EdSAP data to output file --- c
      do 888 IEL=1,nnode_tot
         write(50,1001) (U(IEL,indx,1),indx=1,6)
 888  continue
c
c --- open files with Ke etc. for reading --- c
      CALL NOPEN (NT8,'KE  ')
      CALL NOPEN (22 ,'CSL ')
c
c ------------ start loop for total number of elements ------------ c
      c = 0.d0
      if (NELEM.ne.nel_tot) then
      stop ' terminal '
      else
      continue
      endif
      DO 100 NE = 1,nel_tot ! START LOOP FOR ALL ELEMENTS
c
c --- read element stiffness matrix
      READ (NT8,END=400) ((E(I,J),I=1,ND),J=1,ND)
c --- read element number, connectivity and coordinates
      READ (22,END=500)  IDE,II,JJ,KK,LL,
     &             XYZ(1,1),XYZ(2,1),XYZ(3,1),
     &             XYZ(1,2),XYZ(2,2),XYZ(3,2),
     &             XYZ(1,3),XYZ(2,3),XYZ(3,3),
     &             XYZ(1,4),XYZ(2,4),XYZ(3,4)
       write(51,1002) ide,ii,jj,kk,ll

c --- extract element displacement vector Ue --- c
      do 101, inode=1,4
      if (inode.eq.1) ndnum=II
      if (inode.eq.2) ndnum=JJ
      if (inode.eq.3) ndnum=KK
      if (inode.eq.4) ndnum=LL
      do 102, idof=1,6
      index=((inode-1)*6)+idof
      Ue(index) = U(ndnum,idof,1)
 102  continue
 101  continue




c --- calculate {Ue}'[Ke]{Ue} --- c
```

```
      UeKeUe=0
      do 201, irow=1,ND
      UeKeUerow=0
      do 202, jcol=1,ND
         UeKeUerow = UeKeUerow + Ue(jcol)*E(jcol,irow)
 202  continue
         UeKeUe = UeKeUe + UeKeUerow*Ue(irow)
 201  continue
      UeKeUe = UeKeUe/(X(NE)**penal)
c --- write information to plot_ent file
      write(52,1003) X(NE),(X(NE)**penal)*UeKeUe ! write x and strain energy to file
c --- calculate compliance --- c
      c = c + (X(NE)**penal)*UeKeUe
c --- calculate sensitivity of compliance --- c
      if (UeKeUe.lt.0.d0) write(*,*) 'Negative strain energy: ',UeKeUe
      dc(NE) = -penal*(X(NE)**(penal-1.d0))*UeKeUe
      if (dc(NE).gt.0.d0) write(*,*) 'Positive derivative : ',dc(NE)
 100  CONTINUE ! END LOOP FOR NUMBER OF ELEMENTS
c
c ------------ end loop for total number of elements ------------ c
c --- close binary files --- c
      CALL FCLOSE(22)
      CALL FCLOSE(NT8)
c --- write dc and X to OLD dc and X --- c
      do 300,NE=1,nel_tot
         dcold(NE)=dc(NE)
         XOLD(NE)=X(NE)
 300  continue
c --- filter sensitivities --- c
      call filter(nelx,nely,rmin,X,dc,dcold)
c --- design update by optimality criteria method --- c
      call optcrit(nelx,nely,XOLD,X,volfrac,dc)
c --- postprocessing for output --- c
      vol=0.d0
      chmax=0.d0
      do 301, ii=1,nel_tot
         vol=vol+(XOLD(ii)/dble(nel_tot))
         if ((dabs(X(ii)-XOLD(ii))).gt.chmax)
     &   chmax=dabs(X(ii)-XOLD(ii))
 301  continue
      write(*,1000) iloop,c,vol,chmax,penal
c
      close(50)
      close(51)
      close(52)
c-----------------------------------------------------------------------c
c      if (engEvalString(iep, 'plot_disp;pause(0.5)') .ne. 0) then
c       write(6,*) 'engEvalString failed'
c         stop
c      endif
c-----------------------------------------------------------------------c
 1234 CONTINUE ! END OF CRAIG'S OPTIMIZATION LOOP ...
c
      pause
```

```
c-----------------------------------------------------------------------c
c --- close Matlab Session --- c
c      write(*,*)'--- closing matlab '
c      istatus = engClose(iep)
c      if (istatus .ne. 0) then
c         write(6,*) 'engClose failed'
c         stop
c      endif
c      write(*,*)'--- closing matlab complete '
c-----------------------------------------------------------------------c
      STOP
c --- format statements --- c
 400  STOP ' I/O ERROR ON NT8 '
 500  STOP ' I/O ERROR ON U22 '
C
 1000 format ('It.:',1i3,'  Obj.:',
     + 1e11.6,'  Vol.:',1f9.6,'  ch.:',1f9.6,'  penal:',1f9.6)
 1001 format (6e14.6)
 1002 format (5i5)
 1003 format (2e14.6)
      stop
      end
c#######################################################################c
c#######################################################################c
      subroutine filter(nelx,nely,rmin,X,dc,dcold)
      IMPLICIT REAL*8 (A-H,O-Z)
      PARAMETER (NXT=10000,NU1=40000,NU2=6,NU3=10) ! EL, NODES, DOF, LC
      PARAMETER (ND=24)                            ! DIM OF STIFFNESS MAT

      REAL*8 X(NXT)
      REAL*8 dc(NXT)
      REAL*8 dcold(NXT)

      REAL*8 XMAT(nely,nelx)
      REAL*8 dcMAT(nely,nelx)
      REAL*8 dcoldMAT(nely,nelx)
c --- arrange X, dc and dcold in matrix form --- c
      icount=0
      do 100, icol=1,nelx
         do 101, irow=1,nely
            icount=icount+1
            XMAT(irow,icol)  = X(icount)
            dcoldMAT(irow,icol) = dcold(icount)
            dcMAT(irow,icol)    = 0.d0
 101  continue
 100  continue
c --- filter sensitivities --- c
      do 200, ii=1,nelx-1  ! NEO STIFFENED
      do 201, jj=1,nely
         sum=0.d0
         imink=max((ii-rmin),1)
         imaxk=min(ii+rmin,nelx)
         iminl=max((jj-rmin),1)
         imaxl=min((jj+rmin),nely)
```

```
         do 202, kk=imink,imaxk
         do 203, ll=iminl,imaxl
            xii = dble(ii)
            xjj = dble(jj)
            xkk = dble(kk)
            xll = dble(ll)
            xfac = rmin - dsqrt((xii-xkk)**2.d0 + (xjj-xll)**2.d0)
            sum = sum + dmax1(0.d0,xfac)
            dcMAT(jj,ii) = dcMAT(jj,ii) +
     &       (dmax1(0.d0,xfac)*XMAT(ll,kk)*dcoldMAT(ll,kk))
 203     continue
 202     continue
         dcMAT(jj,ii) = dcMAT(jj,ii)/(xMAT(jj,ii)*sum)
 201  continue
 200  continue

      ii=32+1
      do   jj=1,nely
        dcMAT(jj,ii) = dcoldMAT(jj,ii)
      enddo

c --- arrange XMAT, dcMAT and dcoldMAT into vector form --- c
      icount=0
      do 300, icol=1,nelx
         do 301, irow=1,nely
            icount=icount+1
            dc(icount) = dcMAT(irow,icol)
 301  continue
 300  continue
c
      end
c#########################################################################c
c#########################################################################c
      subroutine optcrit(nelx,nely,XOLD,X,volfrac,dc)
      IMPLICIT REAL*8 (A-H,O-Z)
      PARAMETER (NXT=10000,NU1=40000,NU2=6,NU3=10) ! EL, NODES, DOF, LC
      PARAMETER (ND=24)                            ! DIM OF STIFFNESS MAT

      REAL*8 X(NXT)
      REAL*8 XOLD(NXT)
      REAL*8 dc(NXT)
c --- user inputs --- c
      xl1=0.d0     ! lagrange multi low
      xl2=1.d5     ! lagrange multi high
      xmove=0.2d0  ! move limit
      xdamp=1.d0/2.d0 ! damping value
      nel_tot=nelx*nely
c ---
c --- calculate the new X vector based on heuristic scheme --- c
      do 100, iloop=1,1000
         xldiff = xl2-xl1
c --- START if loop for bisection of lagrangian multi --- c
         if (xldiff.lt.1.0d-4) goto 200
         do 101, ii=1,nel_tot
```

```
            xlmid = 0.5d0*(xl2+xl1) ! lagrange multi mid
            xmax=XOLD(ii)*((-dc(ii)/xlmid)**xdamp)
            xmvup=XOLD(ii)+xmove
            xsolid=1.d0
            xmvlo=XOLD(ii)-xmove
            xempty=1.0d-2
      X(ii)=dmax1(xempty,dmax1(xmvlo,dmin1(xsolid,dmin1(xmvup,xmax))))
 101  continue
c --- calculate mid point for lagrangian multi --- c
         sumx=0.d0
         do 102, jj=1,nel_tot
            sumx=sumx+X(jj)
 102  continue
         volreq=volfrac*dble(nelx)*dble(nely)
         if (sumx.gt.volreq) then
            xl1=xlmid
         else
            xl2=xlmid
         endif
c --- end main loop --- c
 100  continue
c --- END if loop for bisection of lagrangian multi --- c
 200  continue
      end
c#########################################################################c
c#########################################################################c
```